INTELLIGENT SPOT WELDING QUALITY MONITORING USING ADVANCED SIGNAL PROCESSING TECHNIQUES

WANG XINGJUE

NATIONAL UNIVERSITY OF SINGAPORE
2015

INTELLIGENT SPOT WELDING QUALITY MONITORING USING ADVANCED SIGNAL PROCESSING TECHNIQUES

WANG XINGJUE

B.Sci. (Hons.), Nanyang Technological University

A THESIS SUBMITTED

FOR THE DEGREE OF MASTER OF ENGINERRING

DEPARTMENT OF ELECTRICAL AND COMPUTER ENGINEERING

NATIONAL UNIVERSITY OF SINGAPORE

2015

DECLARATION

I hereby declare that this thesis is my original work and it has been written by me in its entirety. I have duly acknowledged all the sources of information which have been used in the thesis.

This thesis has also not been submitted for any degree in any university previously.

Wang Xingjue

18/10/2015

Wang Xingjue

Contents

Acknowledgment

First of all, I sincerely thank my dissertation advisors Prof. Pang Chee Khiang, Justin, and Dr Zhou Junhong from A*STAR Singapore Institute of Manufacturing Technology for their supervision, patience, and inspiration. They provided strong supports and valuable advice when my research was stuck. I am grateful to their consistent guidance and help.

Secondly, I would like to thank Mr. Pan Dayou from A*STAR Singapore Institute of Manufacturing Technology for his help on the welding experiments.

Summary

Resistance spot welding is one of the most important and widely used metal joining techniques in industry. Among different researches in spot welding, the research on quality evaluation stands out as one of the most important aspects. Traditional quality testing of spot welding is destructive, time-consuming, and expensive. In existing literature, many online non-destructive test schemes have been proposed using neural networks (NN), linear vector quantization, SVM methods, finite element modeling, *etc.* However, the proposed online monitoring methods require measurements of physical parameters such as electrical signal, electrode displacement, electrode force, *etc.*, and are vulnerable to changes in experiment conditions. In general, the proposed methods either involve complicated physical models which require much computing power or suffer from the black-box drawbacks of NN.

The aim of this thesis was to find out a fast, convenient, and cheap online monitoring method. For this reason, only the easily obtainable

electrical signals were made use of. In this thesis, a quality classification scheme and quality estimation scheme were proposed. For the proposed quality classification scheme, windowed feature extraction was firstly applied to reduce the dimension of raw data and computational load. The features extracted were RMS voltage, RMS current, and dynamic resistance calculated from RMS current and voltage. A modified SOM was then used to classify the samples into no weld, good weld, and weld with expulsion. The classification was fast and accurate for stainless steel. However, the classification cannot handle the changes in experiment conditions such as welding time variations. As such, for the proposed quality estimation scheme, variation of welding time was introduced and more aspects of quality were considered. The heat affected zone (HAZ) size and nugget size were checked. As boundary of weld nugget was very blurred, the HAZ was chosen as the indicator of quality.

In the feature extraction part, a modified recurrent neural network (RNN) was utilized to extract the peak values of dynamic power. The method can extract all the peaks and has good tolerance to welding time variations. The features used in this part were the peak dynamic power and dynamic resistance at the instant of peak power. After feature extraction, a sliding window RNN was implimented to estimate the HAZ size of welds. To speed up the training process, a modified back-propagation algorithm

was proposed. The accuracy of the proposed method was higher than the multi-layer NN and was able to estimate the HAZ growth curve. This showed great potential to deal with the problem of welding time variation. Next, a SOM-type classifier was used to classify samples into weld with and without expulsion. The accuracy of this method could reach up to 93.3%.

In summary, the proposed method only used the easily obtainable and cheap electrical signals and was able to classify the expulsion conditions of the samples and estimate the HAZ size. The proposed methods also showed good tolerance to changes in experimental condition such as welding time variations.

List of Figures

List of Tables

Chapter 1

Introduction

1.1 Introduction to Spot Welding

Resistance spot welding was firstly invented in 1877. Nowadays, due to its advantages of fast speed, low cost and flexibility, it has become one of the most important welding technique and is widely used in manufacturing industry [1]. Taking automotive industry as an example, a car can have thousands of welds [2].

Resistance spot welding is usually used to join metal sheets. In welding, two tongs of electrodes are pressed to clamp the welded metals together. A high current is then directed through the metals. As the resistance in the faying surface is higher than the resistance in the surface between the

electrodes and metal, more heat will be generated in the faying surface that the welded metals will be joined together.

1.2 Introduction to Spot Welding Quality Monitoring

Quality examination is one of the most important aspects of spot welding. Traditionally, destructive tests were commonly used as the quality examination method. To performance a destructive test in a manufacturing factory, the assembly lines should be suspended. Samples of welds were then picked up randomly and sent through various testing devices or methods such as peel tests, chisel tests, tensile tests, or instrumented tests, *etc.* [2]. Using the destructive test, weld nugget size, heat affected zone (HAZ) width, penetration depth or mechanical strength can be obtained and the quality of the welded sample can be assessed [3]. In general, the destructive test is easy and flexible. However, it is very time-consuming and expensive.

To overcome these weaknesses, many online non-destructive test schemes have been proposed [3]. The principle of the non-destructive test schemes is to firstly monitor the signals such as electrical signals, electrode displacement signals, electrode force signals or ultrasound wave

signals during the welding without any disturbance to the welding process. The signals are then processed to infer the quality. This way of quality evaluation is very fast and convenient and the quality of each samples can be determined right after they are welded. Due to the strengths in pattern recognition and nonlinear fitting, artificial intelligence was frequently applied for non-destructive quality testing. In 1991, an on-line monitoring model using a multi-layer neural network (NN) as a self-organisational structure was proposed [4]. The application of Hopfield NN was introduced in [6] to classify the weld quality based on dynamic resistance. The authors in [7] employed LVQ and used the dynamic resistance profile to perform nugget quality classification.

Even though the proposed methods all achieved satisfactory accuracies, their shortcomings are obvious. The most obvious is the requirement of measurements of many physical parameters such as electrical signals, electrode displacement signals, and electrode force signals. The requirement of many sensors can incur remarkable expenses. Furthermore, the traditional online test schemes were vulnerable to changes in experiment conditions because of negligence of dynamic welding process. In particular, welding process involves interaction of many physical parameters such as dynamic resistance, electrode pressure, and dynamic energy, but traditional methods ignored these effects with the direct application of NN. The

consequence is that the scheme may not work when the experimental conditions such as welding time and welding machine are changed.

1.3 Objectives of the Project

Due to the limitation of the existing methods, the following objectives are expected to be achieved in this thesis.

- To make use of only the electrical signals. The sensors should be cheap and flexible.
- To classify the general weld quality with the input electrical signal.
- To estimate the size of HAZ through the input signals with high accuracy. Both the classification and estimation should be able to deal with varying welding times.

In summary, the aim is to minimize the monitoring cost and develop the most efficient feature extraction and analysis methods. As a consequence, more aspects of weld quality can be determined. The quality evaluation can be more accurate and reliable. In additional, the dynamic property of welding process should also be used such that when the welding time is changed, the proposed scheme is still effective.

1.4 Scope of Proposed Methods

In this thesis, the voltage signal was measured simply by connecting two tongs of the welding machine to the data acquisition system. The current was measured by a Rogowski coil. The measurement setup can be conveniently implemented on the welding equipment without any influence to the primary circuit of the welding equipment.

The obtained raw data was usually very large which caused great difficulty in data processing. For that reason, feature extraction was very necessary to reduce the dimension of input data. For feature extraction, the priority was to find out all the peak positions since the features used in this thesis required the determination of each half cycle. Two peak extraction methods were explored. The first method extracted the crest and trough in each period iteratively using a moving window of predetermined length. The second method applied a feed-forward recurrent neural network (RNN). With the second method, all the peak positions can be determined simultaneously. It is also able to extract the peaks from signal of varying period.

Using the extracted features, various NN models were explored for quality classification. A classification method using fast Self-Organizing Map (SOM) was proposed and was capable of classifying the samples into no weld, good weld, and weld with expulsion rapidly and accurately.

However, this method was not able to deal with problems of welding time variation. As such, a sliding window RNN was designed. The NN can slide along the time series and estimate the HAZ size of each moment. In the meantime, a SOM-type classifier was applied to the times series to check the expulsion condition at each instant. The SOM-type classifier can recognize the possible expulsion features by comparing the similarities and differences between the samples with and without expulsion. With the help of the sliding window RNN and the SOM-type classifier, both the HAZ size and the expulsion condition can be determined even when the welding time is varied. Besides, the HAZ size growth curves of each sample were estimated and corresponded well to the results reported in existing literature.

To verify the performance of the proposed schemes, welding experiments were conducted. The details will be shown in Chapter 3 and Chapter 4.

1.5 Organization

The thesis consisted of five chapters. The first chapter was the introduction. In the second chapter, a literature review discussing welding quality standards, formation of weld nugget, effects of welding current and welding time on quality, signals and features, and the artificial intelligence models used for quality classification was provided. In Chapter 3, the scheme of

windowed feature extraction and SOM-based classification was proposed. The welding experiments to varify the proposed scheme was described in detail with the results and discussion. In Chapter 4, an improved scheme was proposed using RNN-based feature extraction and sliding window RNN and SOM-type classifier based quality estimation. The experiment setup as well as results and discussions were discussed in detail to varify the improved scheme. The last chapter was the conclusion and future work.

Chapter 2

Literature Review

In this chapter, an introduction was given to welding quality standards. Nugget formation during welding was then discussed. Following the discussion of nugget formation, the effects of welding current and welding time on quality, and the signals and features by other researchers were then presented. In the last part, the already-existing artificial intelligence models were elaborated in detail.

2.1 Welding Quality

Welding quality evaluation is one of the most important aspects in research on spot welding. In general, the quality of welding can be categorized into no weld, under-sized weld, good weld, and expulsion [11]. When the current is not sufficient, no weld and under sized weld may occur resulting in small

or even no nugget. On the contrary, if excessive input energy is supplied to the welded pieces, melted metal may be expelled from the weld pool by the heat which leads to expulsion phenomenon. Expulsion is a very common fault during spot welding. It can occur both at the electrode-sheet interface and the faying surface. Many problems can be associated with expulsion such as porosity in the nugget, contaminant on the faying surface, small nugget size, wastage of energy, *etc.* [12].

In addition, a more direct and convenient way of indicating the quality of the weld through the nugget size is preferred in existing literature. According to the relevant British Standard recommends, the minimum nugget size is considered as equation $d = 5\sqrt{t}$ where t is the sheet thickness in mm and d is the weld nugget diameter [13]. Nugget size can be affected by many factors, such as welding time, current, pressing force, surface condition, *etc.*

Finite element modeling is very powerful used in predicting the nugget formation. It is also able to predict the nugget growth as well as the effects of various factors to the nugget size [20, 21, 22]. However, due to the complexity of the welding process, this method requires the determination of many physical parameters and the computation load is usually time consuming. Another very important alternative method is the artificial NN. Compared with finite element modeling, it is more simple

and straightforward. Complex modeling is avoided with the black box and universal approximation properties of NN. However, any information of the welding process is completely neglected which makes this method vulnerable to changes in experiment conditions.

2.2 Welding Nugget

In spot welding, nugget formation is very important in the welding process. It directly determines the mechanical property of the welded pieces such as tensile strength and shear strength. Furthermore, the forming of nugget also affects the porosity condition of the welded pieces. A nugget is formed in the faying surface when enough heat is generated. For nugget formation, the melting of metal firstly happens in some spots on the faying surface [23]. The number and location of spots are determined by the surface condition, input current, and pressing pressure. The spots then expand and merge together. Interestingly, the spots and melting of metal all appear in the peripheral rather than in the center of the contact zone.

The nugget grows very quickly in the first few cycles but the growth slows down in the subsequent cycles. A cavity can form after the solidification of the nugget due to bubbles trapped in the nugget or rapid shrinkage of the nugget during cooling [23].

The actual nugget growing process can be different for various welding materials. For galvanized steel, a zinc coating on the steel substrate can make the welding process more complicated. Because the melting point of zinc coating is 30% lower than the steel substrate and the boiling point is 60% lower than the melting point of steel substrate [24], the melting of zinc will occur first. After the complete melting of zinc, the melted zinc will be extruded from the centre accompanied by the melting of the steel substrate. Some zinc may remain trapped in the nugget region. According to [25], the whole welding process can be divided into eight regions.

In [25], an initial steep fall can be observed due to the break of insulting film and surface asperity covering the substraction in Region 1. The melting of insulting film and surface asperity can increase the contact area significantly. In Region 2, a short rise of dynamic resistance follows due to the heating of zinc Fe-Zn alloy on the electrode substrate interface and faying interface. The heat will raise the dynamic resistance but is not high enough to melt the alloy. In Region 3, the melting of zinc coating on both interface causes the dynamic resistance to fall again. In Region 4, the bulk heating of substrate will dominate the effect of melting of zinc coating and cause the dynamic resistance to increase. In Region 5, a short fall will appear again because of the formation of seal on both surfaces. The seal can continue increasing the contact area. In Region 6, the rise

of dynamic resistance is almost linear which is caused by the heating of bulk material and iron-to-iron interface. In Region 7, due to the melting and softening of the material, the welded pieces will be pushed closer and with broader contact area. As such, the increase of dynamic resistance due to the heating of bulk material will be gradually overridden. The dynamic resistance will reach a maximum and start to fall gradually. In Region 8, if melted material is expelled from the nugget abruptly, a sharp drop of dynamic resistance will appear in the dynamic resistance curve. The generalized dynamic resistance curve of galvanized steel is shown in Figure 2.1.

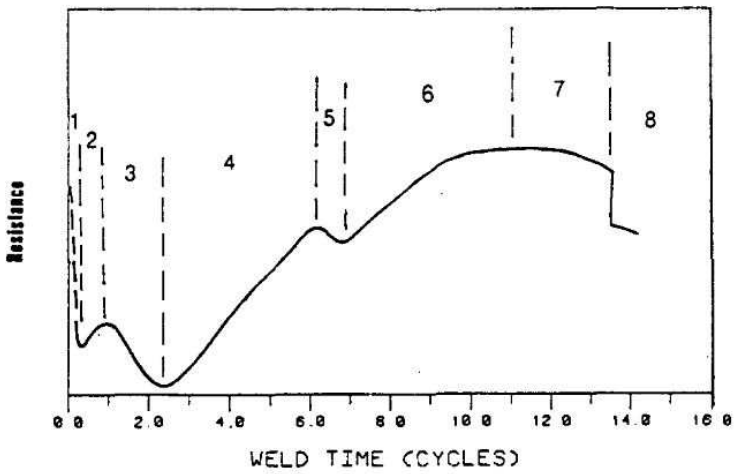

Figure 2.1: Generalized dynamic resistance curve of galvanized steel [25].

Around the nugget, there is an area in the welded pieces where the microstructure is altered by the fast heating and cooling [26]. The area is known as the heat affected zone (HAZ). The metal in that area has not

been melted due to less heat generated. In general, the welded area consists of three distinct microstructural zones known as the fusion zone (nugget), the HAZ, and the base material as shown in Figure 2.2.

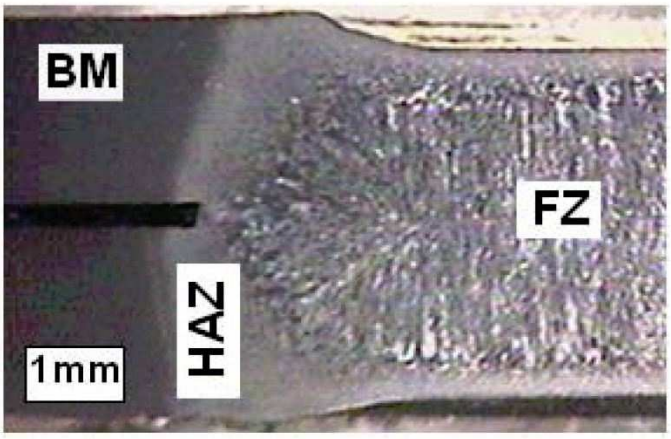

Figure 2.2: The three microstructural zones of of welded low carbon steel piece [26].

2.3 Effects of Welding Current and Welding Time on Quality

The effects of various parameters such as welding current or welding time have been studied extensively. The study showed that the parameters had a great influence on the weld quality [27, 28, 29]. Taking the study of AISI 316L Austenitic Stainless Steel as an example, the following subsections show the effects of welding current and welding time on nugget size,

penetrations depth, HAZ, electrode indentation depth and mechanical performances [29].

2.3.1 Weld Nugget Size

In general, according to

$$Q = I^2Rt, \tag{2.1}$$

where Q is the heat input, I is the current, and R is the dynamic resistance, longer welding time t or larger welding current I leads to higher heat input resulting in larger weld nugget. The effects of welding current and welding time on weld nugget size are shown respectively in Figure 2.3a and Figure 2.3b.

From Figure 2.3, it is shown that the nugget size increases with increase of welding current or welding time but the rate of increase keeps declining due to the reduction of electrical resistance [30]. The declining increase rate may also be due to an expulsion resulting in increase of heat loss to the environment.

2.3.2 Weld Penetration Depth

The effects of welding current and welding time to the weld penetration depth are shown in Figure 2.5a and Figure 2.5b. From Figure 2.5a and Figure 2.5b, it can be observed that the penetration depth increased with

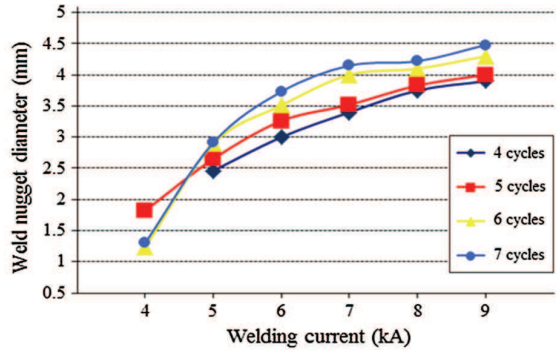

(a)

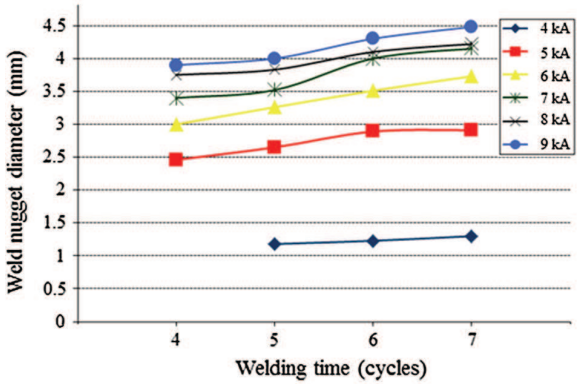

(b)

Figure 2.3: Effects of (a) welding current and (b) welding time to weld nugget size [29].

longer welding time. However for welding current, the penetration depth experienced a sharp drop for 9 kA. The drop of penetration depth for excessive current was caused by the expelling of melted metal by expulsion.

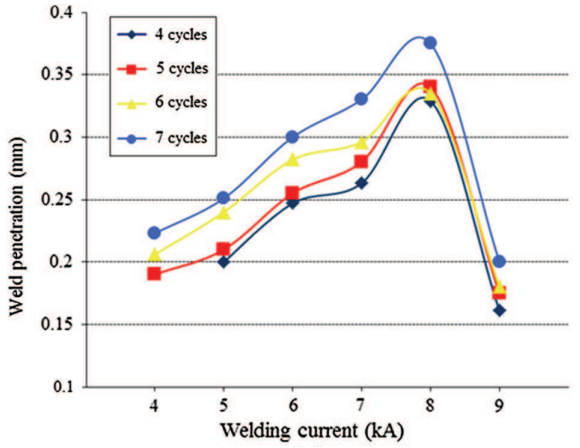

(a)

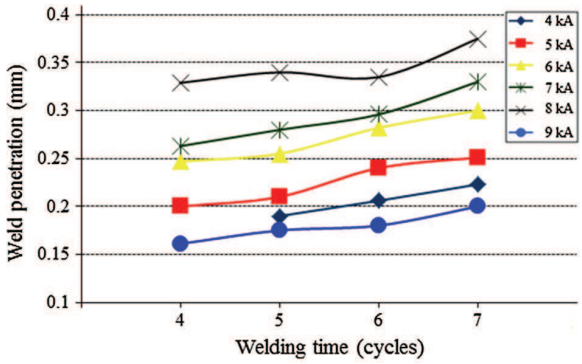

(b)

Figure 2.4: Effects of (a) welding current and (b) welding time to weld penetration [29].

2.3.3 Heat Affected Zone

The heat affected zone (HAZ) is a region around the weld nugget induced by the passage of current and heat dissipation from the weld nugget. The microstructure in HAZ is altered by the heat but the heat is not sufficient to melt the metal. Similar to the weld nugget, the HAZ width increases with increase of welding current and welding time as shown in Figure 2.6a and Figure 2.5b.

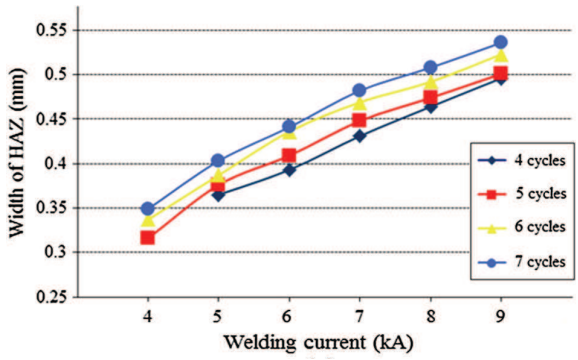

(a)

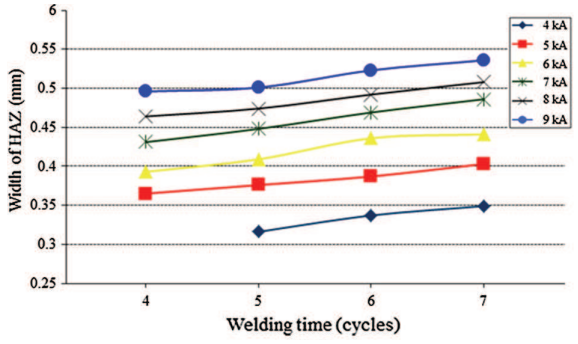

(b)

Figure 2.5: Effects of (a) welding current and (b) welding time to HAZ width [29].

2.3.4 Electrode Indentation Depth

The weld indentation depth is determined by the the electrode pressure and state of the welded pieces. The input heat in the electrode-sheet interface can induce softening of the HAZ and melting of the metal in the fusion zone. With an increase of the input heat, the degree of plastic deformation in the electrode-sheet interface can be increased under electrode pressure. For that reason, the increase of welding current and welding time can lead to increase of indentation depth as shown in Figure 2.6a and Figure 2.6b.

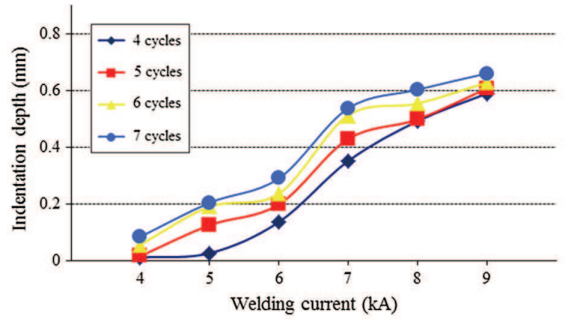

(a)

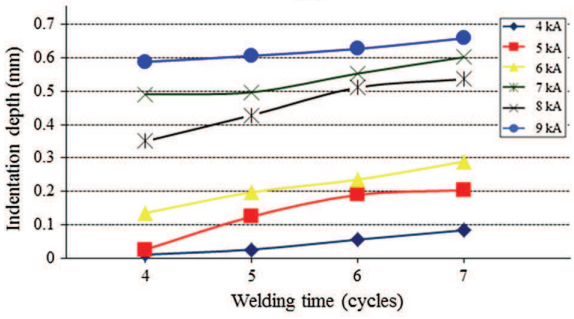

(b)

Figure 2.6: Effects of (a) welding current and (b) welding time to indentation depth [29].

2.3.5 Mechanical Performances

The mechanical performance of the welded pieces are influenced by many parameters such as nugget size, weld penetration, ductility of welded region, and internal discontinuity [29]. Among all the parameters, the nugget size is considered as the dominant parameter by many researchers. For example, the peak load is strongly correlated to the nugget size. As shown in Figure 2.7a and Figure 2.7b, the relationships between the peak payload and the welding current and time are very similar to the relationships between the nugget size and welding current and time. The peak payload increases with the increase of welding current and time. However, for a welding current of 9 kA, the peak payload has a sudden decline because of expulsion.

Besides the peak load, the failure mode is also affected by the welding current. The failure modes of the welds of equal four cycle welding time with welding current ranging from 4 kA to 9 kA are shown in Figure 2.8. The failure mode ranges from solely interfacial fracture mode for 4 kA to completely tearing around the welded nugget and the HAZ for 9 kA. The various failure mode with their corresponding welding current are shown in Figure 2.8.

As shown in Figure 2.8, when the current was in range of 4 kA to 5 kA, the fracture of the weld by tensile test happened in the interface leaving

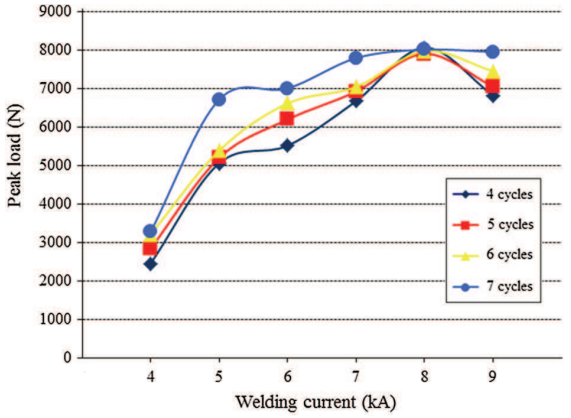

(a)

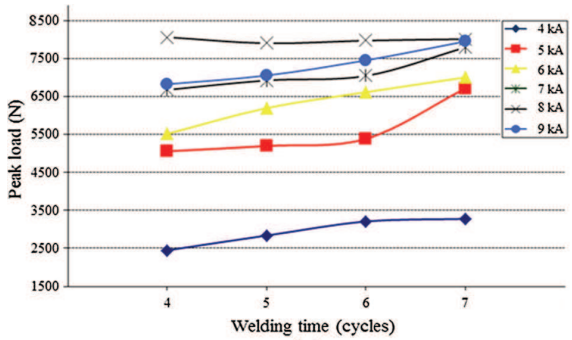

(b)

Figure 2.7: Effects of (a) welding current and (b) welding time to peak payload [29].

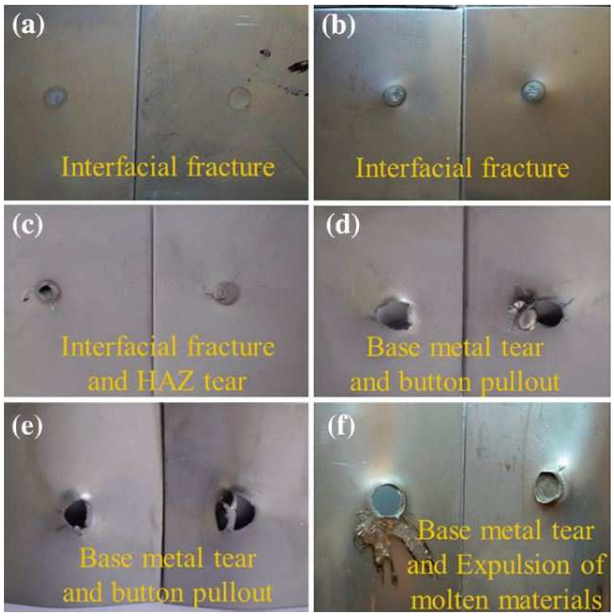

Figure 2.8: Various failure modes and their corresponding current. (a) Welding current of 4 kA; (b) Welding current of 5 kA; (c) Welding current of 6 kA; (d) Welding current of 7 kA; (e) Welding current of 8 kA; (f) Welding current of 9 kA [29].

half of the nugget in one sheet and the other half in the other sheet. The tensile-shear force increased with larger weld nugget but the tensile-shear force was not high enough to be accepted as a good weld. When the current was increased to 6 kA, the separation happened both through the welded nugget and HAZ. With the current in range of 7 kA to 8 kA, the tear took place through both the HAZ and base metal around the welded nugget. The weld nugget was completely torn from one of the sheets. This failure mode was called button pull out [31, 32, 33]. With a current of 9 kA, the weld failed only in the HAZ due to excessive grain growth and softening of HAZ by excessive heat input resulting in reduced textile-shear force [32].

For welding current larger than 6 kA, the weld was considered as good quality using the tensile-shear force.

2.4 Signals and Features for Weld Quality Monitoring

In order to monitor the quality of spot welding online, signals during the welding process are required. Current, voltage, dynamic resistance, electrode displacement, electrode force and optical image are commonly used signals [34]. Different ways of combination of signals have been explored to classify the quality of welded pieces. Among the various signals, the electrode force and electrode displacement, and dynamic resistance were found to provide the most significant piece of information pertaining to the nugget formation. For electrode force and electrode displacement, they are very useful in expulsion detection. During experiments, a clear variation can be observed at the moment of expulsion. As for the dynamic resistance, it is not only useful in expulsion detection but also helpful in estimation of nugget size.

2.4.1 Electrode Displacement and Force

Electrode displacement and force are very useful mechanical signals for quality monitoring, especially for expulsion detection [11, 37]. The electrode displacement refers to the relative movement of electrode tip and electrical force refers to the the force between the electrode tips and the work piece. They are both excellent reflections of thermal expansion of welding process. In addition, the displacement and force signals are sensitive to expulsion. It has been reported that in the case of expulsion, the expelling of melted metal will cause the work pieces to be forced closer to each other. As such, a sharp decrease of displacement and force can be induced and strong variation of both signals can be detected. However, the degree of change can vary with different materials.

The electrode displacement and electrode force signals are usually measured by fiber-optic sensors or piezoelectric sensors, respectively [38]. To avoid disturbance from environment and ensure accurate measurements, the sensors are required to be placed as close as possible to the electrodes. Typical examples of electrode displacement and electrode force signals are shown in Figure 2.15a and Figure 2.15b.

Compared to the dynamic resistance, the electrode displacement signal and electrode force signal characterize the expulsion phenomenon better.

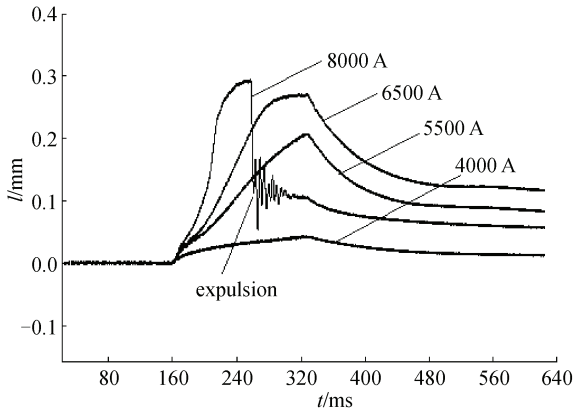

(a)

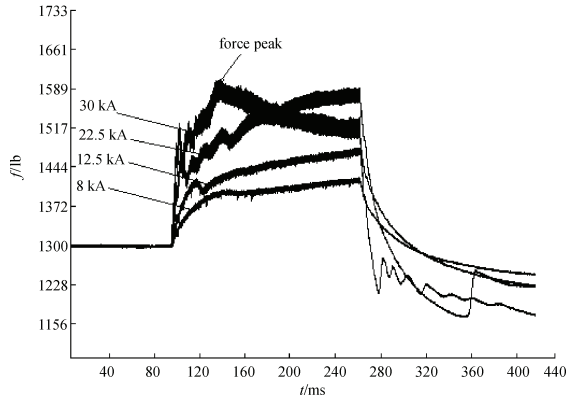

(b)

Figure 2.9: Typical examples of (a) electrode displacement and (b) electrode force signals [37].

However, it has a strict demand for stable working condition and the cost of the sensors are also higher.

2.4.2 Dynamic Resistance Signal and Features

Dynamic resistance is a very important indicator of the welding process. The resistance will change with the welding process and is affected by many factors, *e.g.*, contact distance, contact area, temperature of the material and the phase of the material. The total resistance consists of the resistance in the faying surface R_f, the resistance between the welded piece and the electrodes R_{ew}, and the bulk resistance of the metal R_b by [39]

$$R = R_f + 2R_{ew} + 2R_b. \tag{2.2}$$

Usually, the resistance of the faying surface is the dominant one while the other components of resistance can be neglected. As a consequence, the resistance can be easily calculated from the voltage and current data.

Due to the advantages of the dynamic resistance, dynamic resistance is considered by many researchers as an important feature to predict the quality of the welds. Dynamic resistance is calculated from the current and voltage signals. The current signal is usually measured by Rogowski coil due to its advantages of fast response to changing current, high accuracy, low cost, endurance of large overloads, wide range of

current measurement, flexibility, nonintrusive property, wide bandwidth, and safety. The Rogowski coil was invented by Walter Rogowski. A typical Rogowski coil is made of long helical wire bent into circle and the wire is returned from the center axis of the toroid to the starting point. It is powerful in measurement of alternating current and high speed current pulses because of its fast responses to the changing current with high accuracies [8]. During measurement, the coil is placed encircling the wire. The voltage that is induced is proportional to the rate of change of measured current according to Faraday's law and Ampere's law [9]. The Rogowski coil is always accompanied by an integrator. A simple example of RC integrator is shown in Figure 2.10 [10].

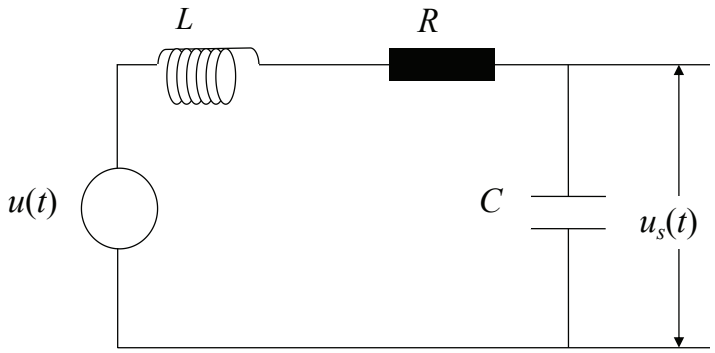

Figure 2.10: Circuit of a simple RC integrator.

In Figure 2.10, L, R, and C are the self-inductance, resistor, and capacitor of the integrator, respectively. The output of the integrator is

proportional to the current at low frequencies following

$$u_s(t) = \mu \frac{NA}{S_m} \frac{1}{RC} I(t), \tag{2.3}$$

where μ is a constant, $u_s(t)$ is the output of the integrator, N is the number of turns of the coil, A is the area of the cross-section of the coil, S_m is the mean length of the coil, R is the resistance, C is the capacitance, and $I(t)$ is the current.

In addition, other designs such as using microprocessor-based device and operational amplifier have been explored to extend the application of the Rogowski coil.

In the welding process, due to the inductance from the circuit, there is always some phase difference between the current and voltage which makes the calculation of dynamic resistance difficult. The actual current I and voltage V are related by

$$V(t) = L \frac{dI(t)}{dt} + RI(t), \tag{2.4}$$

where L is the inductance and R is the resistance. There are mainly four ways of calculating dynamic resistance [40].

1. Voltage (peak)/Current(peak)

The dynamic resistance is calculated by dividing the voltage by the current both at the peak current position. It is the easiest and most convenient way of calculating the dynamic resistance.

2. V_{rms}/I_{rms}

   The second way is to calculate the dynamic resistance by dividing the root mean square (RMS) voltage V_{rms} by the RMS current I_{rms} within a certain period. Many researchers chose to use half a cycle to compute the RMS values and selected the dynamic resistance of each half cycles as the features for processing. The RMS voltage and RMS current are calculated by $\sqrt{\frac{1}{T}\int_{t_0}^{t_0+T} f^2(t)dt}$, where $f(t)$ represents the collected signals.

3. Least-square method

   The third way is based on the equation $V(t) = L\frac{dI(t)}{dt} + RI(t)$. The equation can be arranged into matrix form as

$$V(t) = \begin{bmatrix} \frac{dI(t)}{dt} & I(t) \end{bmatrix} \begin{bmatrix} L \\ R \end{bmatrix}. \tag{2.5}$$

   As such, it becomes a least-square problem where the second entry of the solution gives the unbiased estimation of dynamic resistance.

The solution is given by

$$\left(\begin{bmatrix} \frac{dI(t)}{dt} & I(t) \end{bmatrix}^T \begin{bmatrix} \frac{dI(t)}{dt} & I(t) \end{bmatrix} \right)^{-1} \begin{bmatrix} \frac{dI(t)}{dt} & I(t) \end{bmatrix}^T V. \tag{2.6}$$

For the estimation of dynamic resistance, a moving window can be applied to the data set without overlapping. Using the least-square method, the dynamic resistance within each frame can be computed and used as the features for the following processing.

4. Recursive least-squares

   Given equation $V(t) = \begin{bmatrix} \frac{dI(t)}{dt} & I(t) \end{bmatrix} \begin{bmatrix} L \\ R \end{bmatrix}$, another powerful tool other than least-square method is the recursive least-squares method. It has the ability to track the time-varied dynamic resistance and mutual inductance along the time series with very high accuracies. In general, based on the recursive least squares algorithm, the tracking uses (2.5)–(2.8) [34, 35].

$$\Phi(t) = \begin{bmatrix} \frac{dI(t)}{dt} & I(t) \end{bmatrix}, \tag{2.7}$$

$$\Theta(t) = \begin{bmatrix} L(t) \\ R(t) \end{bmatrix}, \tag{2.8}$$

$$e(t) = V(t) - \Phi(t)\Theta(t), \tag{2.9}$$

$$P(t+1) = \frac{1}{f}(P(t) - \frac{P(t)\Phi'(t)\Phi(t)P(t)}{f + \Phi P(t)\Phi'(t)}), \tag{2.10}$$

$$\Theta(t+1) = \Theta(t) + P(t+1)\Phi(t)e(t), \tag{2.11}$$

where f is the forgetting factor, V is the voltage, $I(t)$ is the current data at moment t, $R(t)$ is the resistance, and $L(t)$ is the mutual inductance. In this thesis, the Θ is initialized by least-square algorithm using first three hundred data. By using recursive least-squares, the dynamic resistance of each moment can be accurately estimated.

2.5 Artificial Intelligence Models for Welding Quality Classification

Many online non-destructive schemes have been proposed. Neural networks were frequently used because of its strength in feature recognition and non-linear curve fitting [41]. In this section, different kinds of neural networks were discussed in detail.

2.5.1 Multi-Layer Perceptron

One of the simplest and most direct method is by using the multi-layer perceptron. Due to its simplicity, it is very popular and appears in various forms in different research papers.

Using [42] as an example, electrical signals were monitored and acquired as the input and the output layers returned nugget size and nugget height. Only one hidden layer was involved in their design. The testing process showed an average percentage error of nugget diameter and height of less than 5% and 8% and highest percentage error of 10.22% and 16.15%.

Recently, a similar algorithm was applied in [43]. However, different from [42], the input signals were chosen to be current, force, resistance while the output was shear strength. 75% of the 243 experimental results were selected to train the NN with back-propagation algorithm. 25% of the 243 experimental results were selected randomly for testing. The NN used in their report was a multi-layer NN with three layers as shown in Figure 2.11, one input layer, one hidden layer and one output layer. After training, the mean squared error (MSE) of all the testing samples were 0.047896 kN and the overall accuracy reached 95%. Their schemes were simply, accurate and showed great usefulness in robot welding. However, their scheme was vulnerable to changes in experiment conditions.

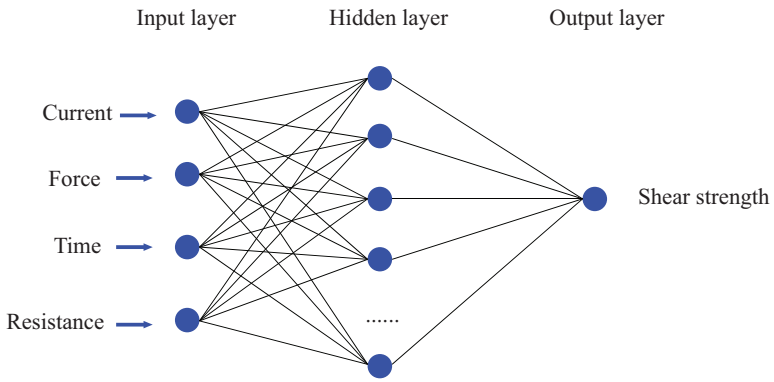

Figure 2.11: The design of multi-layer perceptron.

2.5.2 Neural Networks as a Self-Organisational Structure

Besides the most frequently used standard structure of the multi-layer NN, modification of the multi-layer NN was also explored. The authors in [4] used a NN as a self- organisational structure as shown in Figure 2.12.

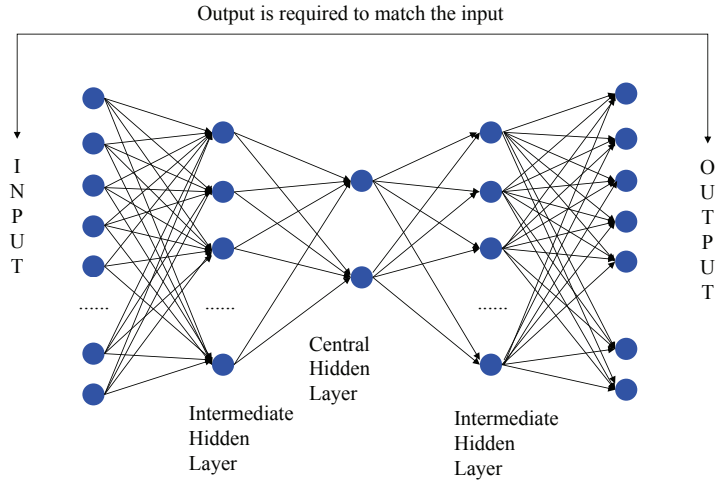

Figure 2.12: The design of the NN as a self-organisational structure.

The NN designed had five layers. There were three hidden layers and the hidden layer in the middle had only two neurons which worked to reduce the dimension of the input set. According to their algorithm, the training process involved only the fifty good welds with resistance data as input. The output was constrained to be the same as the input and therefore the supervision of a teacher can be avoided. In the testing part, five satisfactory and five unsatisfactory welds were used. The classification of all the results are shown in Figure 2.13.

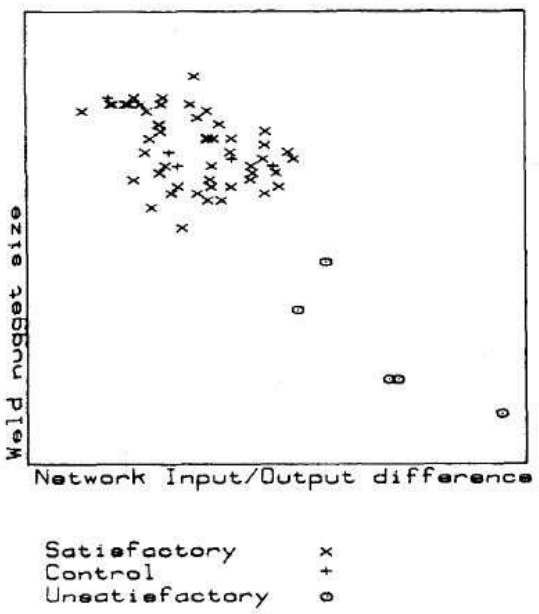

Figure 2.13: Clustering of results [4].

From Figure 2.13, it can be concluded that the fifty-five satisfactory welds formed a cluster and five unsatisfactory welds formed a separate cluster clearly. The quality can be distinguished by checking whether

the difference between input and output layer is in the good cluster. In summary, the auto-associative design simplify the training process. However, the accuracy of this method is not high enough for real application.

2.5.3 Linear Vector Quantization (LVQ) Network

Linear vector quantization (LVQ) network was also applied to classify the quality of spot welding. The work was done in [11] in 2003. LVQ was a precursor of Self-Organizing Maps (SOM) which also applied the winner-take-all approach. The standard structure contains an input layer, a competitive layer, and a linear layer. In the competitive layer each neurons is assigned by a prototype vector which will compete to have a winner that is the closest to the input vector. The linear layer works to associate the winner with the corresponding class. In each iteration, the winner will update its prototype vector to be closer to the input vector if the classification is correct or to be farther away if the classification is wrong.

In their paper, welding voltage, welding current, electrode displacement, and welding force were monitored as candidate features for characterizing expulsion. However, only the amplitude of welding force variation signal was selected due to its effectiveness in identifying expulsion.

The design of the LVQ network is shown in Figure 2.14. In Figure 2.14,

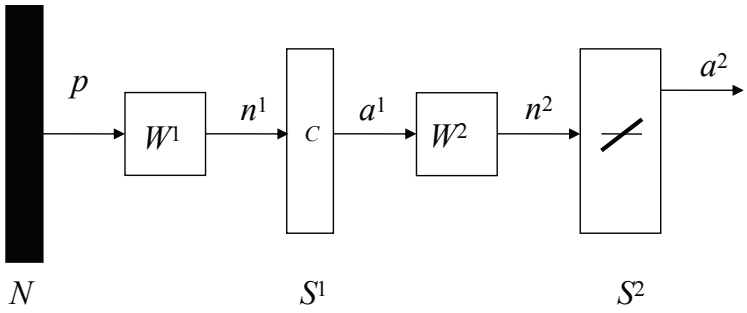

Figure 2.14: The design of LVQ network.

N was the size of the input vector, p was the input vector, W^i was the weight matrix for the i-th layer, S^i was the number of the neurons in the i-th layer, n^i was the net input vector of the i-th layer, and a^i was the output of the i-th layer. There are three neurons in the competitive layer corresponding to three subclasses and two neurons in the linear layer corresponding to two quality conditions (normal and expulsion). Each input vector was constructed by a certain value and its preceding value along the time series of input signal. The network was firstly trained by the input vectors from four measurements with expulsion using one hundred epochs with the basic LVQ learning rule [5]. It was then trained by another one hundred epochs with the LVQ2 learning rule which involved the update of both winner neuron and the next-to-nearest neuron if the input vector $p(i)$ was classified incorrectly.

After the training, signals from another set of thirty measurements were used to test the network. The results showed that all the thirty measurements were classified correctly. Their scheme was accurate and efficient. However, their scheme was restricted by the requirement that the exact expulsion point should be detected accurately along the time series. Furthermore, the sole use of welding force variation signal may not be sufficient for accurate prediction for other materials. The high cost of accurate weld force measurement may also be a problem.

2.5.4 Hopfield Neural Network

A Hopfield NN was applied in [6] for quality estimation. Hopfield neural network was invented by John Hopfield in 1982 as a completely recurrent neural network (RNN) [6]. It showed great usefulness in associative memory and optimization problems.

For the work in [6], the main idea was to recognize and classify different dynamic resistance patterns with the aid of Hopfield network and used the patterns to classify weld quality. Specifically, the dynamic resistance curve was chosen as the input signal. First of all, the dynamic resistance was normalized to between 0 to 1. After that, the dynamic resistance curve was mapped into a two dimensional 6×10 element bipolarized vector with

a default value of -1. An example of the dynamic resistance curve and the mapped vector were shown in Figure 2.15.

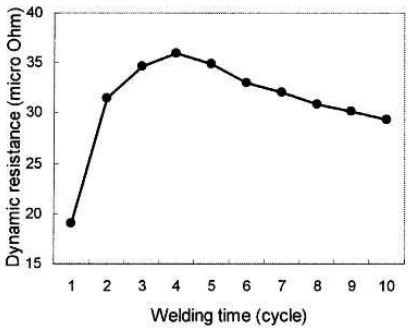

(a)

$$R = \begin{bmatrix} -1, -1, +1, +1, +1, -1, -1, -1, -1, -1 \\ -1, -1, -1, -1, -1, +1, +1, +1, -1, -1 \\ -1, +1, -1, -1, -1, -1, -1, -1, +1, +1 \\ -1, -1, -1, -1, -1, -1, -1, -1, -1, -1 \\ -1, -1, -1, -1, -1, -1, -1, -1, -1, -1 \\ +1, -1, -1, -1, -1, -1, -1, -1, -1, -1 \end{bmatrix}$$

(b)

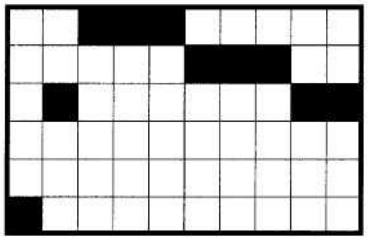

(c)

Figure 2.15: An example of dynamic resistance curve, the mapped vector and graphical pattern [6].

The Hopfield network he applied was a single layer feedback NN with symmetric weights. The number of neurons was set to be the same as the

number of mapped elements. In each iteration, the output of each neuron was updated according to

$$y_i^{k+1} = \text{sgn}(\sum_{j=1, j\neq i}^{n} w_{i,j} y_j^k - \theta_i), \tag{2.12}$$

where k represents the number of iterations, $w_{i,j}$ is the weight of the j-th neuron to the i-th neuron, θ_i is the threshold and $\text{sgn}(f)$ is represented by

$$\text{sgn}(f) = \begin{cases} 1 & \text{if } f > 1, \\ f & \text{if } -1 \leq f \leq 1, \\ -1 & \text{if } f < -1. \end{cases} \tag{2.13}$$

The energy function of the network was shown to be

$$E = -\frac{1}{2} \sum_{i=1}^{n} \sum_{j=1}^{n} w_{i,j} y_i y_j + \sum_{i=1}^{n} \theta_i y_i. \tag{2.14}$$

In the training process, five typical dynamic resistance curves of different welding current ranging from 5 kA to 11 kA were selected as the prototype patterns as shown in Figure 2.16. The weights of the NN were adjusted such that the energy function reached its minimum for all the five patterns. The tensile strength of each pattern were measured representing the quality standard for each pattern. In the quality evaluation part, the input pattern

from a weld was presented to the NN. It was then classified to a certain stored prototype pattern based on the likelihood to each pattern and thus the quality was determined. Ten dynamic resistance patterns of random currents between 6.5 kA and 8 kA were used to test the performance of their network and the result showed an accuracy of about 80%.

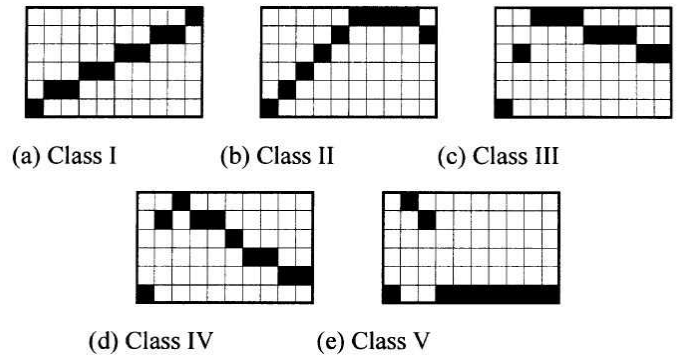

Figure 2.16: The five prototype vectors from welds of different current [6].

2.5.5 Time Series Prediction Using NN

Besides the NN models discussed in the previous sections, various NN models were designed for time series problem. Although these NN models are usually applied in other fields such as financial prediction or climate forecasting [14, 15, 16], they are also very useful for spot welding.

The standard NN method for time series is called the focused time delay NN as shown in Figure 2.17 [17, 18]. It can be considered as an extension of auto-regressive time series modeling. The principle of the NN is to collect

the past time series values and use the value to predict the new value. The training method is standard using the back-propagation algorithm.

An upgrade of the previous method is called the nonlinear autoregressive

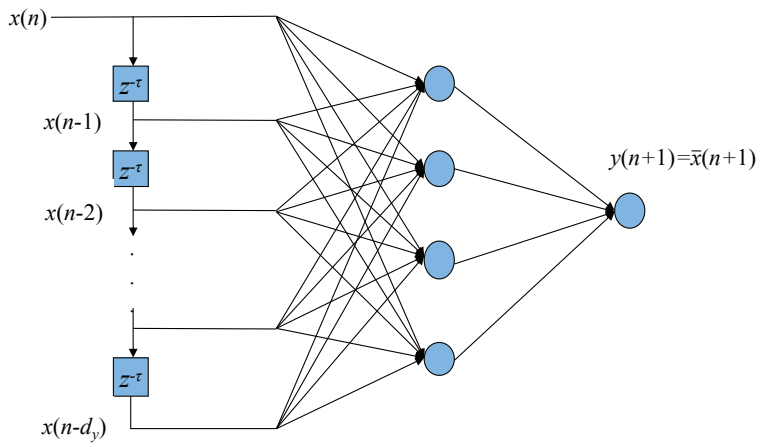

Figure 2.17: The architecture of the focused time delay NN.

models with exogenous input (NARX) RNN [16, 19]. The model involves the previous states as well as inputs. As compared to the time-delayed NN with state function $y(n+1) = F(x(n), x(n-1)...)$, the state function for NARX RNN can be expressed as $y(n+1) = F(y(n), y(n-1)...; u(n), u(n-1)...)$. The network is reported to be very efficient for modeling a non-linear dynamic system [19].

2.6 Summary

In this chapter, the concepts of welding quality, nugget formation, effects of welding current and welding time on quality, signals and features, and

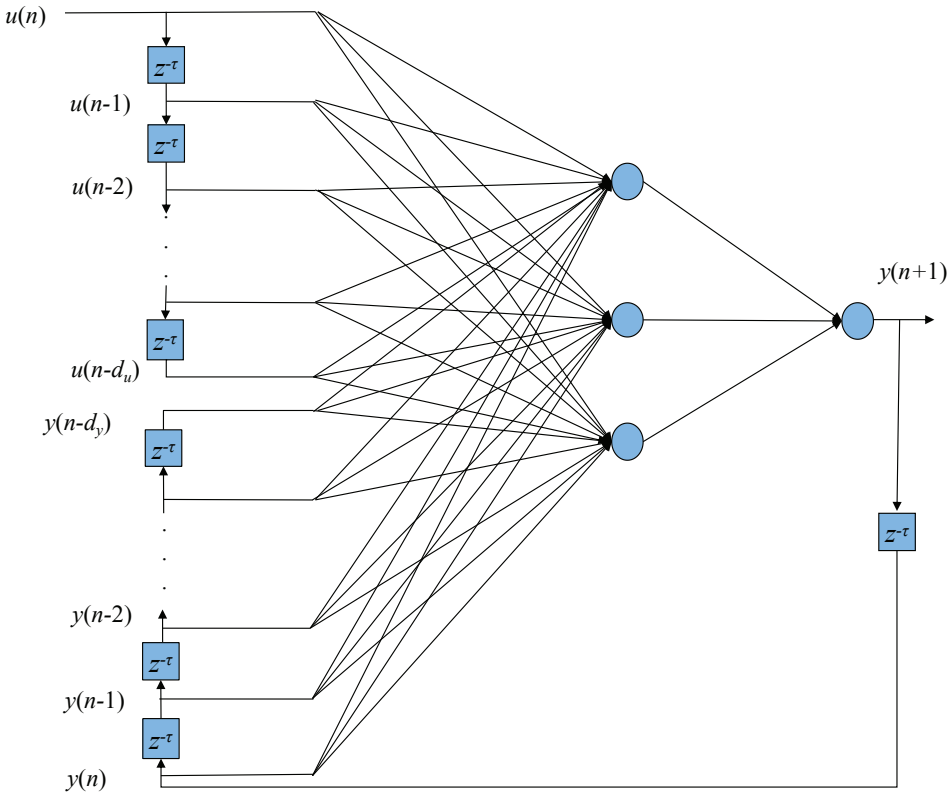

Figure 2.18: The architecture of the NARX RNN.

artificial intelligence models were introduced. Many artificial intelligence models such as multi-layer NN and Hopfield network were discussed. However, they have relatively high computational costs and are vulnerable to changes in experimental conditions.

Chapter 3

Windowed Feature Extraction and SOM-Based Quality Classification

In the previous chapter, signals, features and various artificial intelligence models were reviewed. The already-existing schemes were limited by the shortcoming of the direct use of neural network (NN) and were vulnerable to changes in experimental conditions such as change of welding times. To solve the problem, two schemes were proposed in the thesis. The details will be discussed in the following two chapters.

The first scheme used dynamic resistance calculated by root mean square (RMS) current and voltage of each half cycles as well as the RMS

current and RMS voltage as features. To determine each half cycles, a moving window was used. After that, a self-organizing map was applied to classify the qualities of the welds. The general flow is shown in Figure 3.1.

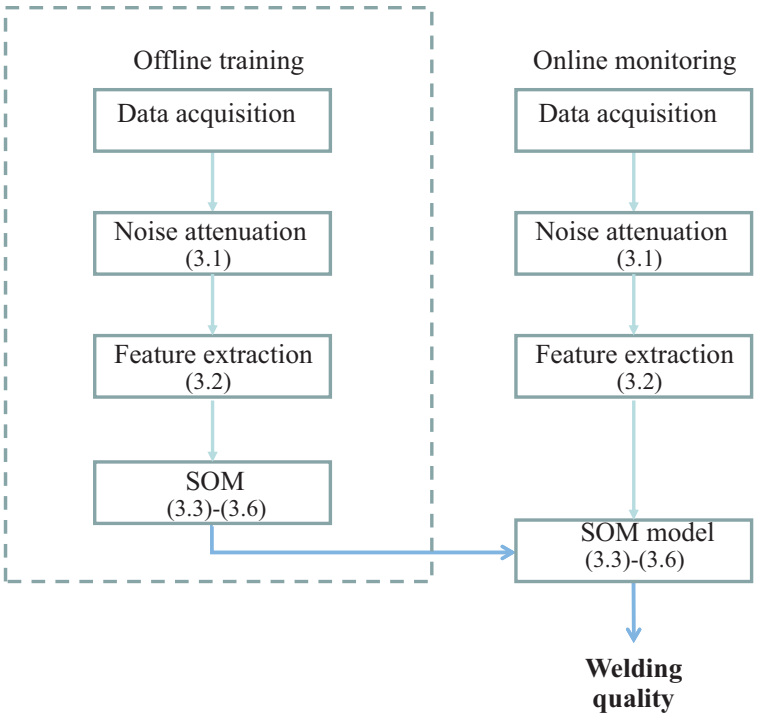

Figure 3.1: Flow chart of the proposed quality classification scheme.

3.1 Welding Quality Classification Framework

In this section, the complete framework of the proposed quality classification scheme is presented. The details of windowed feature extraction and the design of SOM are elaborated.

3.1.1 Signal Pre-Processing

Electrical signals are strongly correlated with nugget formation and can be easily captured. For that reason, many monitoring systems utilize electrical signals for indication of nugget quality. Current and voltage signals were used in this thesis. In particular, dynamic resistance and dynamic power were calculated from the current and voltage signals and used to estimate the quality of welding.

For the proposed quality classification scheme, the current was measured via a Rogowski coil without an integrator. The sampling rate was 10^6 Hz. Due to the high sampling rate and large transient in the circuit, strong noise was observed in the voltage signal. For that reason, the integration and noise attenuation should be done to the raw data before feature extraction.

Raw Data

The measured current and voltage signals were shown in Figure 3.2. The current signal was computed by integrating the voltage signal from the Rogowski coil in Matlab. A linear downward drift of current was observed and solved by drift compensation. From Figure 3.2, it can be seen that the current tends to increase with cycles and voltage tends to decrease with cycles.

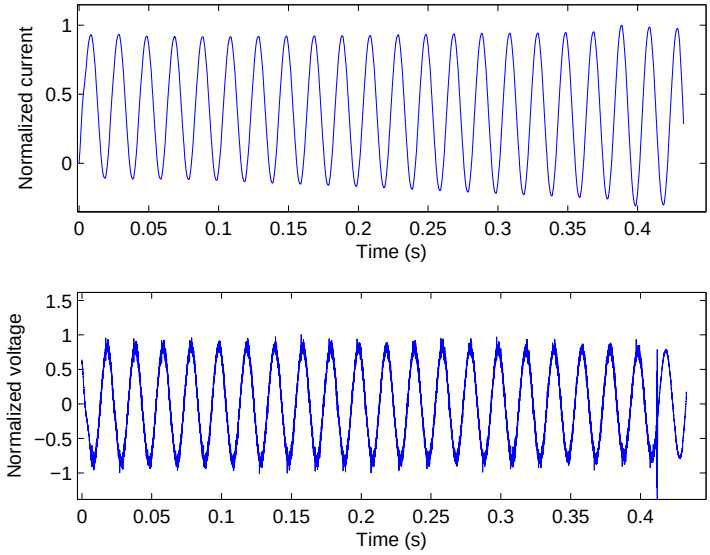

Figure 3.2: An example of current and voltage signals from the experiments.

Noise Attenuation

Due to the high sampling rate and the large transient in the circuit, there was noise observed in the welding signals, especially the experimental voltage signals. In order to suppress the effects of noise on classication, a second order low pass digital Butterworth filter from Matlab toolbox with a 5000 Hz cut-off frequency was used to attenuate the noise in voltage. It allows low frequency signals to pass and attenuates signals with frequencies higher than the cut-off frequency. The gain $|H(j\omega)|$ of the second-order Butterworth low pass filter is expressed in terms of the transfer function *H(s)* as shown in

$$|H(j\omega)| = \frac{H_0}{\sqrt{1 + \left(\frac{\omega}{\omega_c}\right)^4}}, \tag{3.1}$$

where ω_c is the cutoff frequency and H_0 is the gain at zero frequency.

Example of original voltage signal and the filtered voltage signal are shown in Figure 3.3 and it is indicated that the huge noise of the voltage signal is attenuated efficiently with the low pass filter.

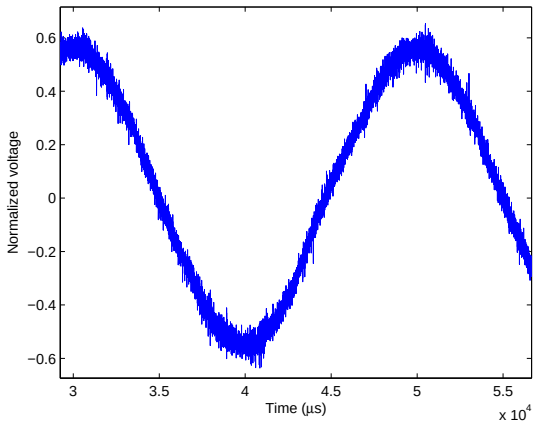

(a)

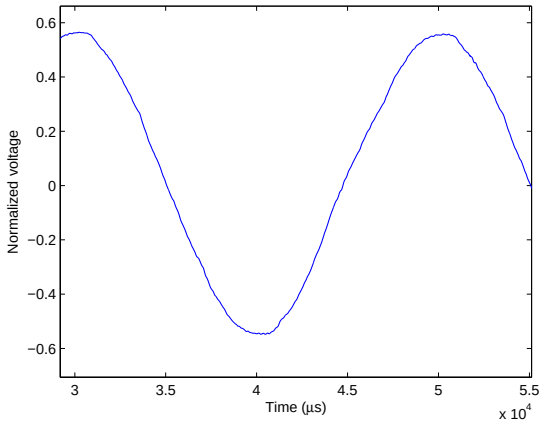

(b)

Figure 3.3: Comparison between the (a) original voltage signal and the (b) filtered voltage signal.

3.1.2 Windowed Feature Extraction

Feature extraction is a very popular and powerful mathematical approach toin time domain signal processing. Usually, the raw data is so huge which makes the interpretation very difficult. However, the important information can be extracted and transformed into lower dimensional space. By using feature extraction, the signal dimension can be effectively reduced, retaining the key information [49]. It relieves much of the burdens of computation. There are mainly five categories of feature extraction methods. They are data descriptive statistics, data descriptive models, time-independent transforms, time series transforms, and domain dependent feature extraction [49]. In this thesis, feature extraction method from data descriptive statistics was used.

For the proposed quality classification scheme, dynamic resistance calculated from RMS current and RMS voltage as well as RMS current and RMS voltage were chosen as the key features. In order to determine the half cycles, the extraction of crests and troughs from current and voltage signals was the primary task. From Figure 3.4, it can be observed that current in the first cycle is severely distorted. The distortion is possibly caused by the large transients in the initial state. Besides, the period of each half cycles as well as the crest values of each half cycles also vary which increases the difficulty of peak extraction. As such, a sliding window

of predetermined length was applied in the proposed quality classification scheme to extract crests and troughs of the signals.

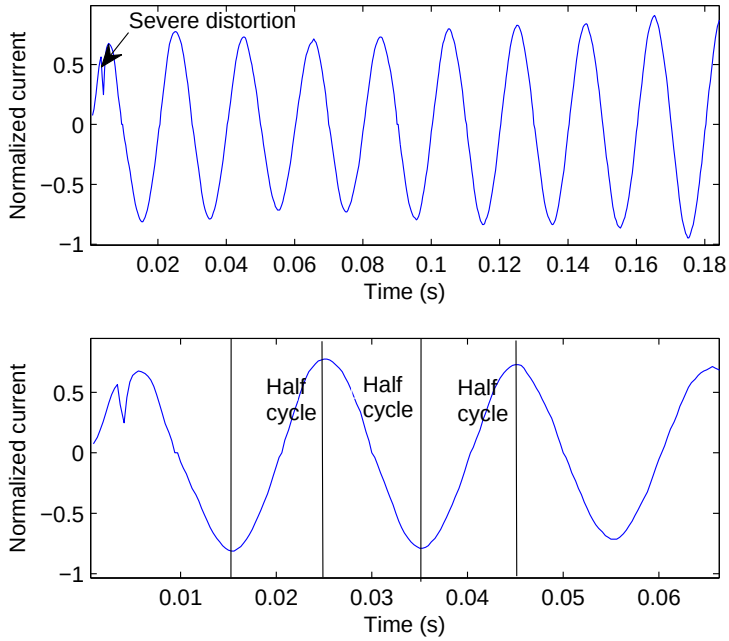

Figure 3.4: An example of half cycles of a signal and signal distortion.

Extraction of Crests and Troughs

For the proposed quality classification scheme, dynamic resistance was calculated by dividing the RMS voltage by the corresponding RMS current. From the signals, it can be observed that the current and voltage were almost in phase. As such, the calculation of the RMS value of the current and voltage in their corresponding half cycles did not incur much error.

Even though the periods varied with each half cycle, the periods of half cycles only varied in a small range between 0.009 s to 0.0102 s. For that

reason, a sliding window with length of 0.02 s(which was almost the period of a full cycle) was used to extract the crests and troughs. This method required a pre-estimation about the total number of cycles. The algorithm was represented by the flow chart shown in Figure 3.5.

The first trough was set to be the minimum point within the first 0.018 s. The first crest was set to be the maximum point within the first 0.018 s. In the subsequent steps, the search for crest started from the previous trough position with a length of 0.02 s. Likewise, the search for trough started from the previous crest position with a length of 0.02 s. The process continued iteratively until all the crests and troughs were determined.

The crest $C(n)$ and trough $T(n)$ can be extracted using

$$\begin{cases} C(n) = \arg\max_{t\in[T(n-1),T(n-1)+0.02]} I(t) \\ T(n) = \arg\min_{t\in[C(n-1),C(n-1)+0.02]} I(t) \end{cases} \tag{3.2}$$

where $I(t)$ is the current signal, $C(n)$ is the n-th crest and $T(n)$ is the n-th trough.

This method is very fast and efficient. The extracted crest and trough positions are accurate. However, it has several drawbacks. First of all, if the distortion in the first cycle is too severe, the wrong choice of starting point can ruin the following extraction process. Due to the variation of welding time, the total number of crests and troughs may not be the same.

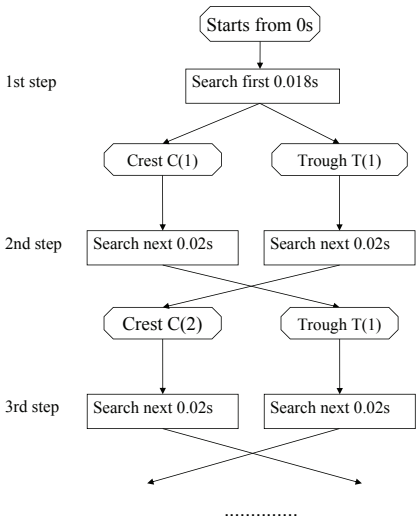

(a)

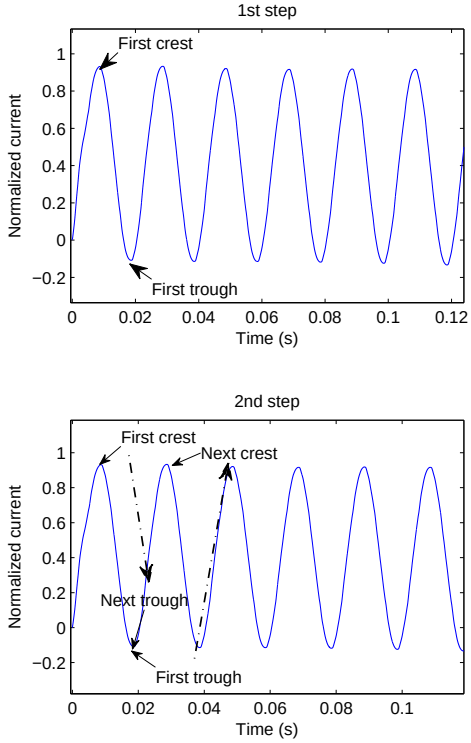

(b)

Figure 3.5: (a) The flow chart representing the sliding window-based crest and trough extraction and (b) a simple example.

As a result, it is likely that the crest or trough in the last cycle may be missed. In addition, this method requires a high consistency in period of half cycles.

Extracted Features

The features employed for the proposed quality classification scheme were the dynamic resistance calculated from RMS current and RMS voltage within a half cycle as well as the RMS current and RMS voltage. A half cycle was determined to be the period between the crest and the adjacent trough position and vice versa as shown in Figure 3.6. The RMS value of both current and voltage in the same half cycles were computed separately. The dynamic resistance was then calculated by dividing the RMS voltage by the corresponding RMS current. The dynamic resistance, the RMS current, and the RMS voltage were then combined to form input vectors for the training and testing of the NN. The input vectors shall be normalized to between 0 and 1 before being fed into NN.

The normalized RMS current, RMS voltage, and dynamic resistance of all the samples from experiments are shown in Figure 3.7. The welding material used in the experiments was stainless steel. From Figure 3.7, it can be interpreted that the dynamic resistance of stainless steel decreased almost monotonously during the whole welding process.

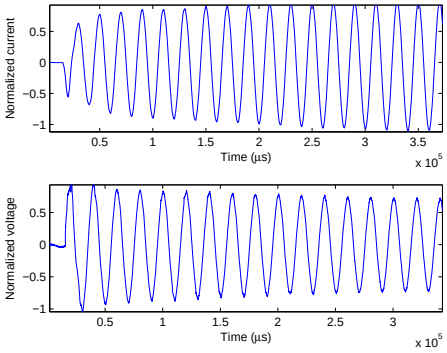

(a)

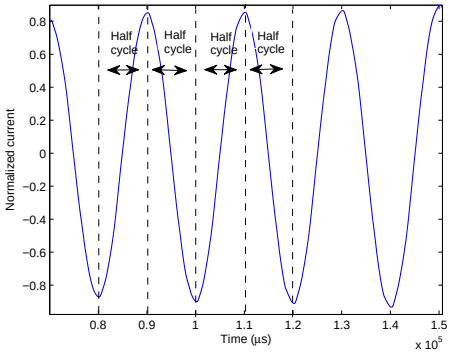

(b)

Figure 3.6: Examples of (a) current and voltage signals and (b) half cycles for feature extraction.

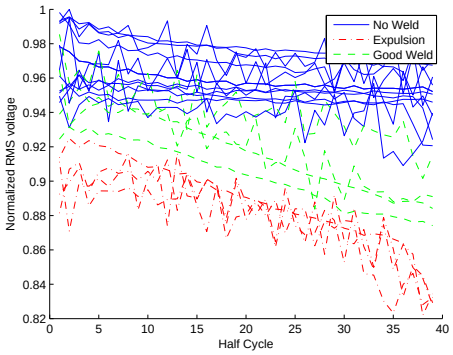

(a)

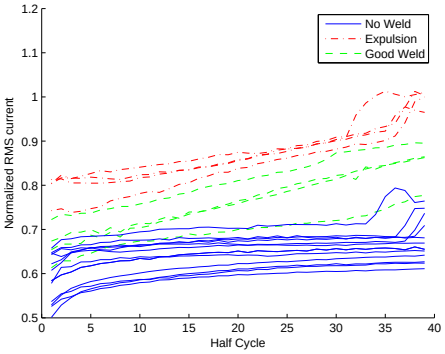

(b)

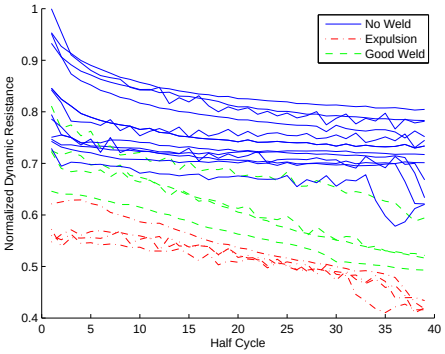

(c)

Figure 3.7: (a) RMS voltage, (b) RMS current, (c) Dynamic resistance curves of all the samples.

3.1.3 SOM for Weld Quality Classification

Self-organizing map is a very useful unsupervised NN proposed by Kohonen [55]. It classifies inputs according to their likelihood through competition process and is very powerful in feature recognition. It possesses both high accuracy and high speed.

The SOM used in the proposed quality classification scheme consisted of four hundreds neurons arranged into 20×20 two-dimensional grid. In the training process, each neuron was assigned a random vector of weight with the same length as the input vector. The input vectors were normalized before fed into the SOM. In each iteration, an input vector was chosen randomly and presented to the NN. The neuron with the smallest Euclidean distance was selected as the winner. The winner together with the neighborhood neurons updated their vectors to be more like the input vector through

$$w(k+1) = w(k) + \alpha(k)\ \Omega(k)(x - w(k)), \tag{3.3}$$

where k is the number of iterations, α is the learning rate with expression $\alpha(k) = \alpha_0 e^{-\frac{k}{T}}$, and T is set to be one thousand [45, 46]. The learning rate is set in this way that it will shrink with iterations to ensure the convergence of the training process. Ω is the neighborhood function which determines

to what extent the vector of the neuron will move towards the input vector. The neighborhood function is Gaussian function related to the Euclidean distance $d_{x,y}$ to the winner via

$$\Omega(k) = e^{-\frac{d_{x,y}^2}{2\sigma(k)^2}}, \tag{3.4}$$

where σ is the topological neighborhood width. To speed up the computing, only neurons within the neighborhood width will update their vectors. The neighborhood width will cover all the neurons initially, and it keeps decreasing exponentially until only immediate neighbors are affected after T iterations. The expression for neighborhood width is shown as

$$\sigma(k) = \sigma_0 e^{-\frac{k}{T}}. \tag{3.5}$$

To speed up the training [47, 48], the learning rate can be adjusted as

$$\alpha(k) = \alpha_0(1 - \frac{k}{T}). \tag{3.6}$$

At the end of the training process, all neurons will be labeled based on the label of the closest input vectors. In this chapter, for the proposed quality classification scheme, the samples were categorized to no welds, good welds, and welds with expulsion. As such, after the training, all the

neurons were labeled "no welds," "good welds," or "welds with expulsion." In the testing part, the trained map were used to classify the quality of the testing samples by labeling samples with the labels of the neurons with the closest distance to their input vectors.

3.2 Experiment and Results

The previous section demonstrates the signal processing and artificial intelligence models which are necessary to non-destructive quality evaluation. Experiments were conducted to test the performance of the proposed two schemes. This section will cover the experiments to verify the proposed quality classification scheme.

3.2.1 Experiment Setup and Procedure

To verify the proposed quality classification scheme, twenty welds were conducted. The welding machine used in the experiments was miller LMSW series portable welding machine as shown in Figure 3.8. The portable welding machine is light-weight and easy to be operated. However, the electrode lacks the water cooling system and thus the heating of the electrodes has remarkable effects to the welding. For the welding machine, the current and voltage of the welding system cannot be varied. The only parameter that can be changed is the welding time. In addition, the welding

is handled manually. The pressure on the specimen may not be consistent as compared with the huge automotive welding machine applied in industry.

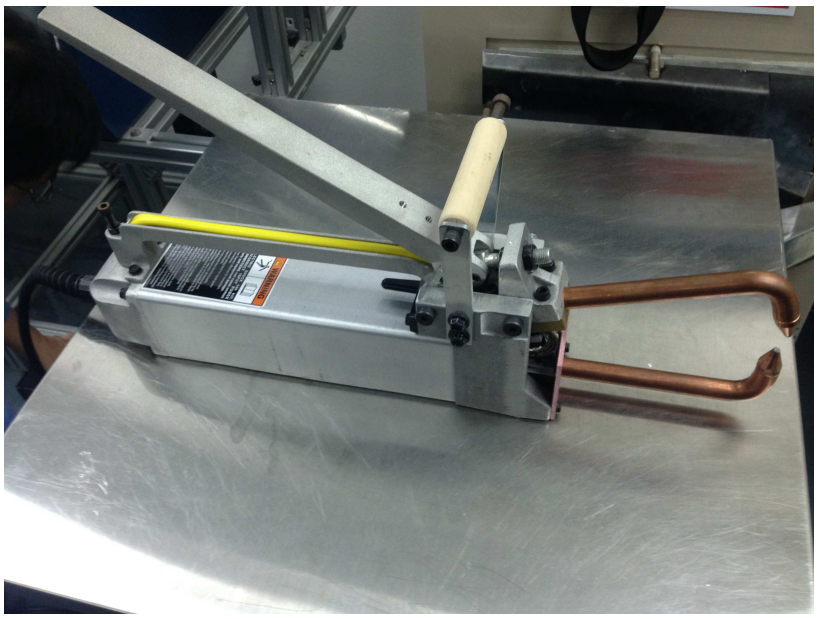

Figure 3.8: A picture of welding machine.

The experiment setup for the proposed quality classification scheme included a welding machine, a voltage and a current sensor, Picoscope and a PC as shown in Figure 3.9. The sampling rate of the Picoscope was 10^6 Hz. The current was measured by Rogowski coil without the integrator and the integration was done by PC. A linear downward drift of current was observed which was resolved by drift compensation. The voltage was measured by connecting the two electrodes to the Picoscope. The measurement setup is shown in Figure 3.10.

The welded samples were chosen to be 3 mm thick stainless steel plates which was 2.5 cm wide and long as shown in Figure 3.11. Twenty welds

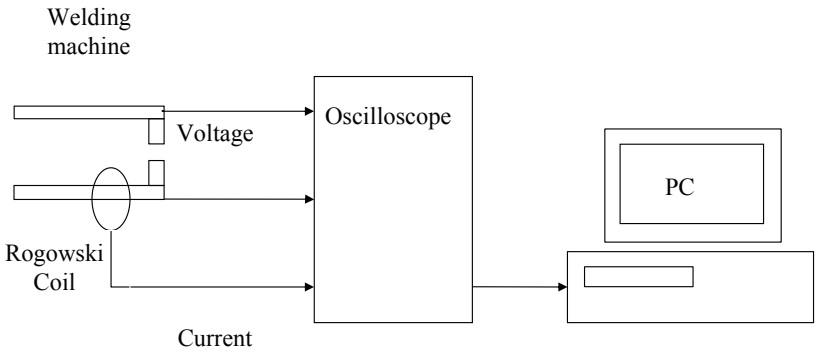

Figure 3.9: Experimental setup for the proposed quality classification scheme.

Figure 3.10: An illustration of measurement setup.

were conducted. The welding time for all the welds was chosen to be 0.3 s. After the welds, the qualities of the samples were examined by destructive tests according to their expulsion conditions. The samples were classified into no weld, good weld, and weld with expulsion.

Figure 3.11: A picture of the samples.

3.2.2 Results and Discussion

The quality categories of each sample after the destructive tests are shown in Table 3.1. Among them, two samples with no weld (Samples 1 and 2), two samples with good quality (Samples 3 and 6) and two samples with expulsion (Samples 10 and 18) were used for training while the rest of the samples were used for testing. The features used in the proposed quality classification scheme were the RMS voltage, RMS current and dynamic

resistance calculated from the RMS voltage and current of each half cycles.

Table 3.1: Quality of samples. Label 0: Sample with good quality. Label 1: Sample with expulsion. Label -1: Sample with no weld (current passing through the corners)

Sample No.	Label	Sample No.	Label
1	-1	11	-1
2	-1	12	-1
3	0	13	-1
4	-1	14	0
5	-1	15	0
6	0	16	-1
7	-1	17	-1
8	-1	18	1
9	-1	19	1
10	1	20	1

In the proposed quality classification scheme, the SOM was chosen for classification. The training process took approximately 17.8 s which was very fast. The classification results were shown in Table 3.2.

From Table 3.2, it can be observed that only Sample 17 was misclassified into good weld. All the samples with expulsion were classified correctly. The overall accuracy was 92.9%. The results showed that SOM not only maintained fast speed, but also sustained high accuracy in classifying no weld, good weld, and weld with expulsion. However, this way of treatment is vulnerable to the changes in experiment conditions such as change of

Table 3.2: Quality classification results by SOM

Sample No.	Estimated Quality	Real Quality
4	-1	-1
5	-1	-1
7	-1	-1
8	-1	-1
9	-1	-1
11	-1	-1
12	-1	-1
13	-1	-1
14	0	0
15	0	0
16	-1	-1
17	0	-1
19	1	1
20	1	1

welding time. For the other working pieces made of galvanized steel or mild steel involving more complex welding processes, this accuracy may not be guaranteed.

3.3 Summary

This chapter described the proposed quality classification scheme. The proposed quality classification scheme mainly consisted of signal preprocessing, windowed feature extraction, and SOM-based quality classification. The signal preprocessing included integration of Rogowski coil voltage, noise attenuation, and feature extraction. For the feature extraction, the features were selected as RMS current, RMS voltage and dynamic resistance calculated from RMS current and voltage. Half cycles were determined with the help of crest and trough extraction using a sliding window of predetermined length. The SOM was then applied to classify the samples into no weld, good weld, and weld with expulsion. Following the developed models, the experiment setup, the procedure and the results of experiments were described in detail. The results showed that the SOM was fast and the overall accuracy reached 92.9%. However, this method was still unable to deal with the problem of changes in welding time.

Chapter 4

RNN-Based Feature Extraction and Sliding Window NN-Based Quality Estimation

In this chapter, an improved scheme is proposed for quality estimation. For the proposed quality estimation scheme, in general, the peaks of dynamic power and the dynamic resistance at the instant of maxima were selected as the features. The peak powers were extracted with the help of recurrent neural network (RNN). After feature extraction, a sliding window RNN was applied to estimate the heat affected zone (HAZ) size, and the SOM-type

classifier was applied to classify the expulsion condition. The general flow is shown in Figure 4.1.

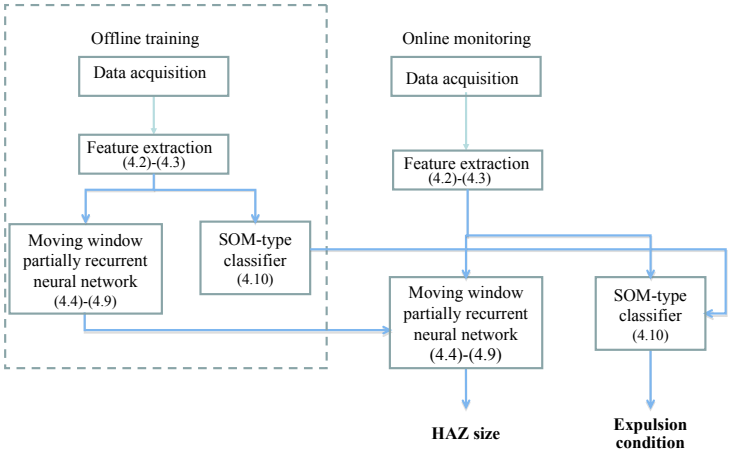

Figure 4.1: Flow chart of the proposed quality estimation scheme.

4.1 Welding Quality Estimation Framework

In this section, the complete framework of the proposed quality estimation scheme is presented. The details of the modified RNN based feature extraction, the sliding window RNN, and the SOM-type classifier are elaborated.

4.1.1 Signal Preprocessing

For the proposed quality estimation scheme, an integrator was implemented in the welding system for measurement of current. Accompanying the integrator, a welding scanner was installed replacing the Picoscope and PC resulting in reduction of the sampling rate. However, the new setup showed very little noise. With the aid of the new setup, the current and voltage data were captured directly. The new setup simplified the signal acquisition and signal preprocessing significantly.

Typical examples of current and voltage signals from the experiments are shown in Figure 4.2. By comparing the current and voltage signals, it can be found that the phase difference between the current and voltage was maximum for the crossing of zero points and minimum for crest and trough positions. However, the phase differences at certain peak positions still existed. The phase difference complicated both the dynamic resistance calculation and the determination of peak position.

4.1.2 RNN-Based Feature Extraction

The features used in the proposed quality estimation scheme were peak dynamic power and dynamic resistance at the instant of peak dynamic power. Due to the phase difference at certain peak positions, the peaks in current did not correspond exactly to the peaks in voltage. This caused

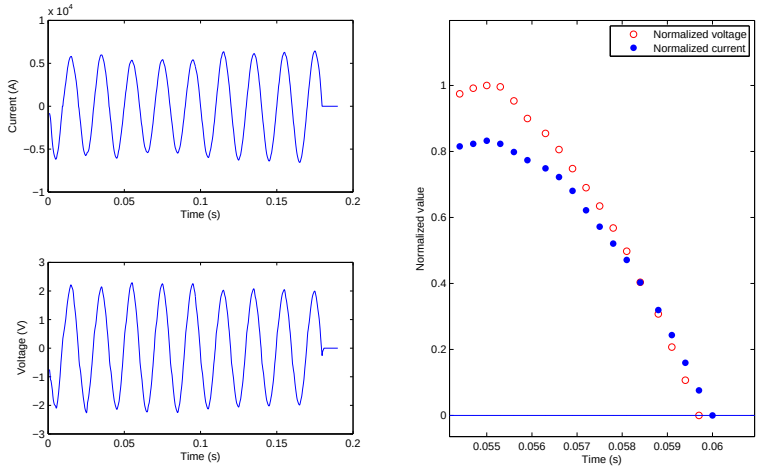

Figure 4.2: An example of current and voltage signals from the experiments.

difficulty both to the determination of peak position of dynamic power and to the calculation of dynamic resistance at that instant. To deal with this problem, the dynamic resistance was calculated firstly by recursive least-square method and the dynamic power was calculated simply by multiplying the current with the voltage as shown in

$$P(t) = I(t)V(t), \tag{4.1}$$

where $P(t)$ is the power. The peak positions of the power were then extracted from the power data, and the corresponding dynamic resistance was chosen for the following processing.

In the field of quality examination of spot welding, dynamic resistance is one of the most commonly used indicators. However, the sole usage of

dynamic resistance may not be sufficient. During the welding, the current and voltage change according to the change of resistance of the work piece and the internal control of the welding system. The welding process involves the interaction of the input power to the material and the property changes of the material.

Peak Extraction by RNN

For the proposed quality estimation scheme, a feed-forward RNN was applied for peak extraction. The peak extraction was done to the dynamic power data rather than the current and voltage. The total number of neurons was set to be equal to the total number of power data. Each neurons were mapped to the power data at each instant as shown in Figure 4.3. The distance between the adjacent neurons was set to one. Each neuron has suppressing effects to the nearby twenty five neurons in the form of synaptic weights. The range of suppressing effect shall be set to be more than a quarter of cycle and less than a half cycle. The synaptic weight of each neuron to the neighboring neurons follows

$$w_{i,j} = -e^{-\frac{d_{i,j}}{15}}, \tag{4.2}$$

where $d_{i,j}$ is the distance between neuron i and neuron j. The output of each neuron is updated through

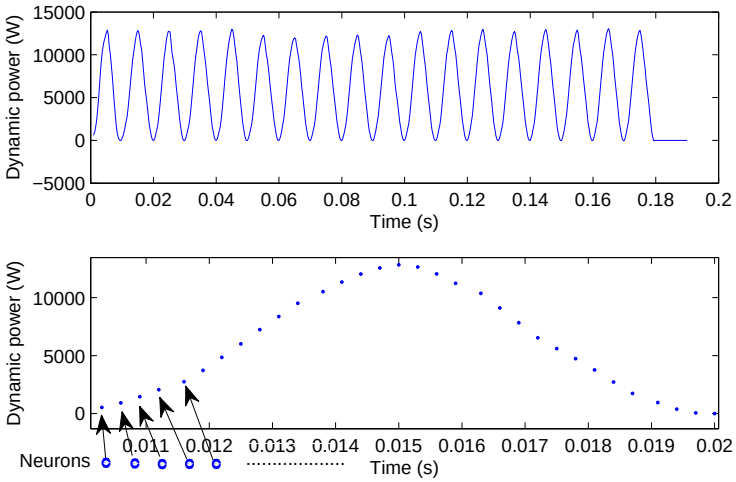

Figure 4.3: The implementation of feed-forward RNN for peak extraction of power data.

$$\begin{cases} \frac{du_j(t)}{dt} = \frac{\delta}{1+exp(-(x_j+\sum\limits_i w_{i,j}u(i)-\theta))}, & \text{if } x_j + \sum\limits_i w_{i,j}u(i) - \theta \geq 0, \\ \frac{du(j)}{dt} = -\delta u(j) & \text{if } x_j + \sum\limits_i w_{i,j}u(i) - \theta < 0, \end{cases} \tag{4.3}$$

where x is the normalized power data corresponding to each neuron and θ is the threshold of each neuron with value of 0.5 [44]. The consequence of the NN is that only the neurons corresponding to peak power will be activated and the rest of neurons are totally deactivated. An example of the neurons' activity after one thousand iterations is shown in Figure 4.4. It can be seen that the peak positions match well with the activated neurons' positions. However, the situation that both two adjacent neurons were activated might occur as shown in Figure 4.5. This was because both of

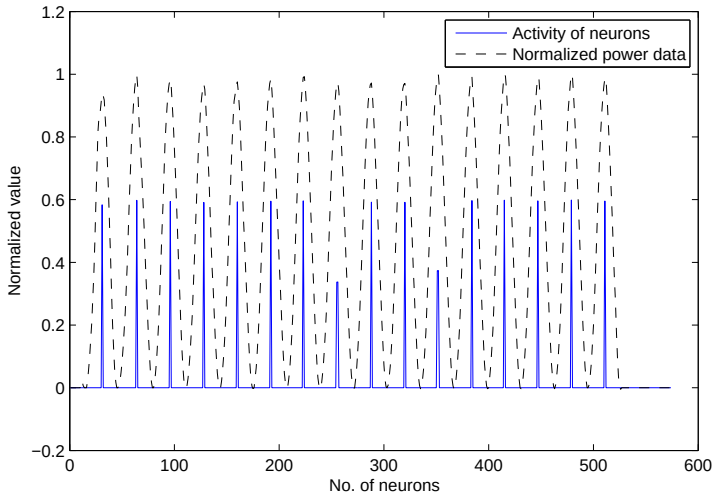

Figure 4.4: The peak extraction results by the feed-forward NN.

the points were too close to the exact peak point, and thus the values of both points were very close to each other. To handle this problem, the first point was chosen as the peak point in peak extraction. With the help

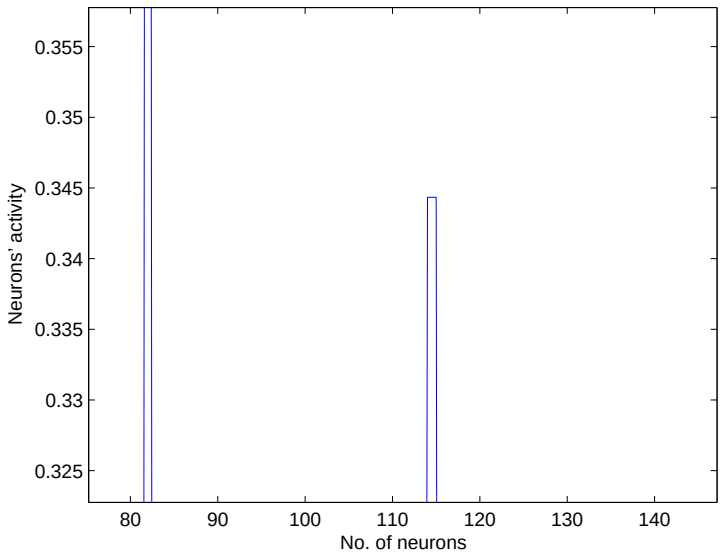

Figure 4.5: An example of the activation of two adjacent neurons.

of RNN for peak extraction, all the peaks can be extracted at one time. It is also capable to deal with signals with variations of periods and peak values.

Extracted Features

For the proposed quality estimation scheme, the features used were peak power and dynamic resistance at the instant of peak power. The dynamic resistance was calculated firstly using the standard RLS algorithm [34, 35]. The comparison between various methods is shown in Figure 4.6. It is shown that RLS algorithm possesses high accuracy and thus the dynamic resistance calculated can be used for training the neural networks.

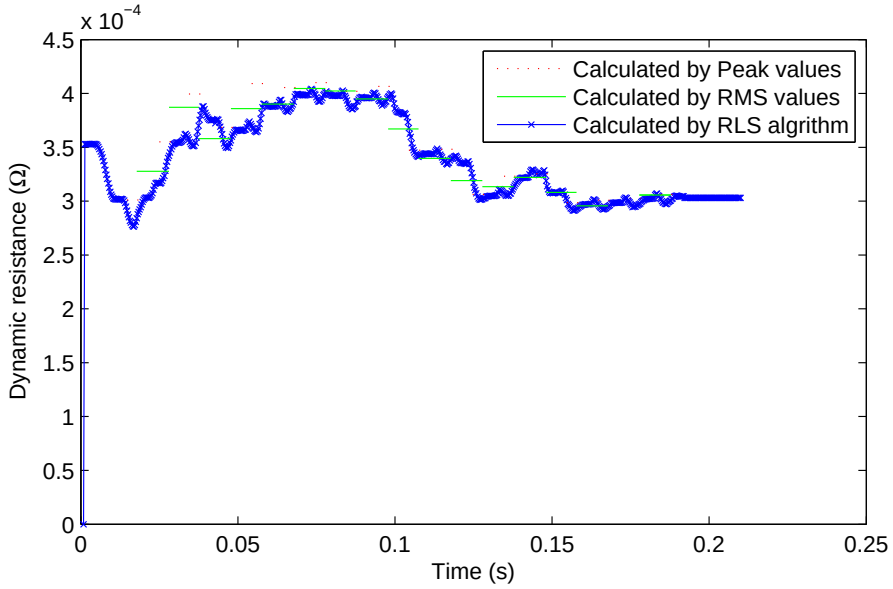

Figure 4.6: Comparison of different methods of resistance calculation.

The dynamic resistance curves of all the samples from the experiments are shown in Figure 4.7. Compared to the dynamic resistance curves from the proposed quality classification scheme presented in previous chapter, the dynamic resistance curves appeared to be more complicated. Typically, in the very beginning of the welding process, dynamic resistance of most samples experienced a sharp drop. A hump of dynamic resistance was then observed within time interval from 0.05 s to 0.12 s. However, the exact dynamic curves varied with samples. From Figure 4.7 it can also be interpreted that the signals of samples with and without expulsion were very similar. It was extremely hard to distinguish the two quality conditions.

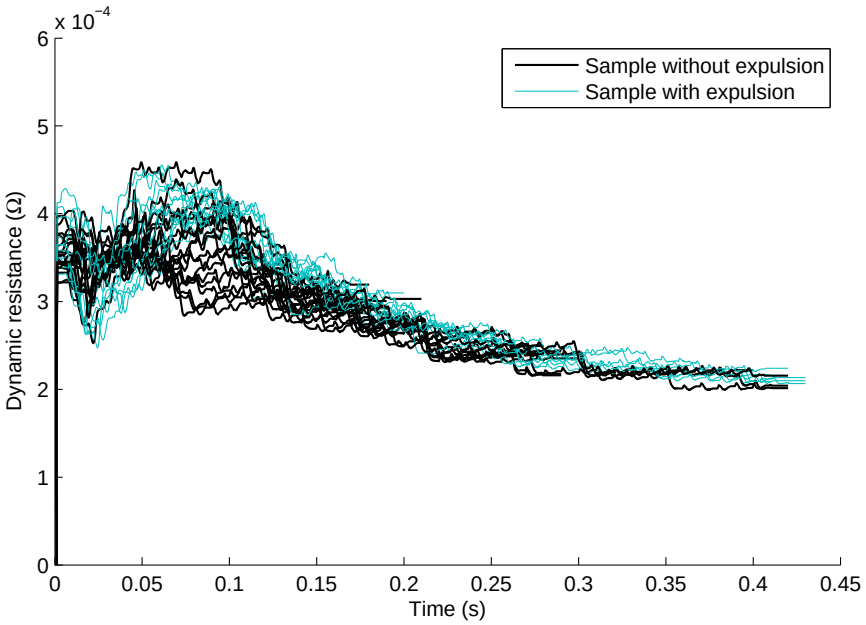

Figure 4.7: Dynamic resistance curves of all the samples for the proposed quality estimation scheme.

Following the peak extraction of power data presented in the peak extraction section, the dynamic resistance at peak power positions was identified. The extracted dynamic resistance and peak power time series data were normalized to between 0 and 1 and presented to the artificial intelligence neural networks as inputs in the following section.

Examples of extracted dynamic resistance curve and peak power curve are shown in Figure 4.8. The general dynamic resistance curves obtained were different from [25]. Recalling the generalized dynamic resistance curve of galvanized steel as shown in Figure 2.1 in Chapter 2, the whole welding process were divided into eight regions. However, these eight regions can not be identified clearly in the dynamic resistance curve from our experiments.

4.1.3 Sliding Window RNN for HAZ Size Estimation

In general, a common way is to feed all the time series data into the NN and train the NN according to the squared error between the outputs of the NN with the desired results. This way of treatment is convenient and straight forward. However, due to the direct use of the NN, the information of the dynamic interaction among various parameters along the time series is totally neglected. The traditional method is too direct forward and it

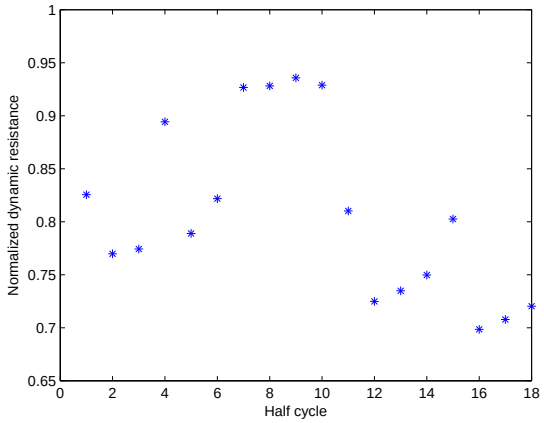

(a)

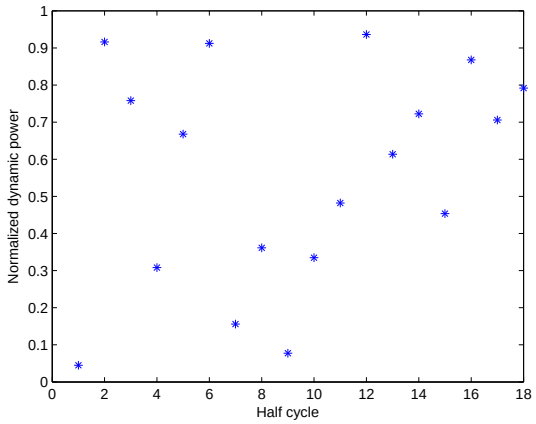

(b)

Figure 4.8: An example of (a) extracted dynamic resistance and (b) peak power points.

may encounter severe problems when dealing with time series problem of varying time lengths.

In order to solve time series problem of varying time lengths, it is intuitive is to make use of a sliding window. As such, a sliding window RNN was proposed. In the process of welding, the dynamic resistance represents the property of the welded piece while the dynamic power reflects the input power from the welding machine to the welded piece. The dynamic resistance and power interact with each other dynamically and mutually determine the nugget growth. Due to the complexity of the welding process, it is very difficult to come up with an exact physical model to formulate the whole interaction. For that reason, NN's black box property and universal approximation capability show great usefulness in this part. In summary, for the design of the NN, the following features are expected to be achieved. They include a sliding window, capability of representing the interaction relationship between the resistance, power, and nugget size, and simple modeling.

The general idea of the sliding window RNN is shown in Figure 4.9. The window covered five adjacent normalized resistance data and power data obtained in the feature extraction part. There was another input called HAZ size. In this chapter, the HAZ was applied instead of nugget size as from the measurement of nugget size, the boundary of HAZ was

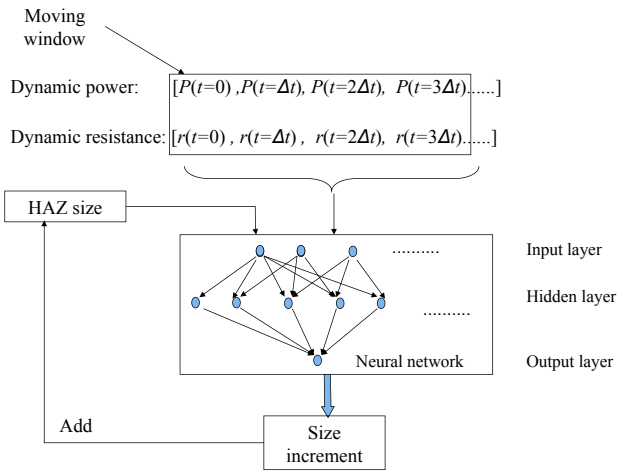

Figure 4.9: The design of sliding window RNN.

much clearer than the nugget zone. The HAZ also had strong correlation to nugget size. The output of the NN was the increment of the HAZ size. The output increment of the HAZ size was added directly to the HAZ size generating the new HAZ size for the next iteration. The HAZ sizes of all the samples were normalized to between 0 and 1. The sliding window RNN achieved the purpose of both representing the dynamic process and avoidance of the complex modeling of their interaction.

In the training process, the times series from training set were presented to the NN in random sequence. The NN slid through the time series and the HAZ sizes at the last moment were compared with the real normalized HAZ sizes for tuning of the weights of the NN. The training was done in

batches. The error function E was the weighted sum of the squared error of all the training samples as shown in

$$E = \sum_{i=1}^{n} \frac{1}{N(i)} (H(i) - \hat{H}(i))^2, \tag{4.4}$$

where n is the total number of training samples, H is the HAZ size, $\hat{H}$ is the estimated HAZ size by the network, and $N(i)$ is the total number of data points of sample i. The reason of the weighted sum is that the training samples have different number of data points and weight factors are needed to avoid bias to the training. As such, the weight factor for each sample was set to be the inverse of the total number of data points. The training was stopped when the error function was less than 0.001.

Traditionally, back-propagation algorithm was commonly used in training. However, it has severe drawback of slow convergence which makes the training very time-consuming [51, 52]. The speed of convergence drops exponentially as the error function becomes smaller. The training usually takes more than half an hour to tune the error function less than 0.001. It is worth mentioning that momentum can be implemented to save the time [53].

To speed up the training process, a modified gradient descent method was proposed in this chapter. Rather than updating the weight directly by

the gradient, speed was introduced and the gradient descent behaved like an attractive force. The new update law is shown as

$$w(k+1) = w(k) + v, \tag{4.5}$$

$$v = v - \alpha\eta\frac{dE}{dw}, \tag{4.6}$$

$$\eta = \frac{1.7/160}{E + 1/160} + 0.3, \tag{4.7}$$

where v is the speed, E is the error function, and η is a variable which controls the influence degree of attractive force to the speed. It is designed that when $E = 1$, $\eta \approx 0.3$, and when E decreases, $\eta \to 0.4$. The learning rate α was also modified such that it kept changing according to the change of error function. If the error function became smaller by the adjustment, the learning rate would be increased according to

$$\alpha = \begin{cases} \alpha(1+\epsilon) & \text{if } \alpha < 2, \\ 2 & \text{if } \alpha \geq 2, \end{cases} \tag{4.8}$$

where $\epsilon \sim$ U(0,0.1). If E became larger, the learning rate would be decreased by [54].

$$\alpha = \alpha(1-\epsilon). \tag{4.9}$$

To avoid the problem of overshooting which is the major concern of this method, a rule is set that the moment the error function becomes larger, the speed is reset to zero. Furthermore, if the error function starts from a huge value, *e.g.*, one thousand, the speed will become so fast that the error function may not converge to the global minimum. To solve this, the traditional back-propagation algorithm is applied for error function larger than ten. In very rare cases, the training may be stuck in the local minimum. Re-initialization of the NN and its speed can be done to deal with this situation.

The comparison of the error function curves between the two algorithm is presented in Figure 4.10a and Figure 4.10b. It is shown that when the error function was smaller than 0.1, for the back propagation algorithm, the decrease of error function slowed down exponentially. However, for the proposed algorithm, on the contrary, the decrease of error function can still speed up in the area where the error function is already very small. Although there existed some bounce-backs of the error function, the error function returned back to its decreasing mode very quickly.

The comparison showed that time consumption of the traditional back propagation algorithm was far more than 10000 iterations while the number of the proposed algorithm was less than 400. This is 25 times faster than the traditional method.

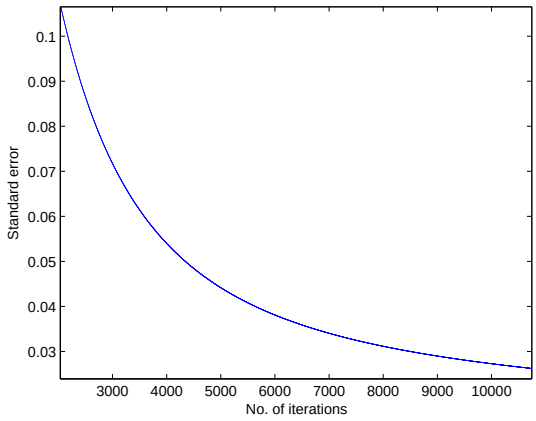

(a)

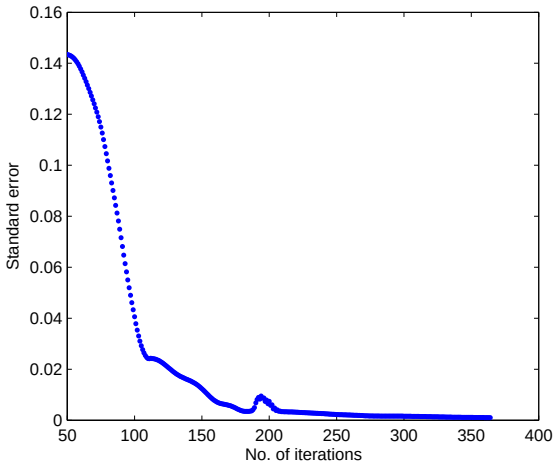

(b)

Figure 4.10: Comparison of the error function curves between the (a) traditional back propagation algorithm and (b) modified back propagation algorithm.

4.1.4 SOM-Type Classifier for Classification of Expulsion Condition

The SOM-type classifier was employed in the proposed quality estimation scheme for expulsion checking. The common way of quality checking uses the whole time series into a certain type of NN, such as multi-layer NN, LVQ or SOM, and then train the NN to assess the expulsion condition. However, this treatment may result in low accuracy due to the following reasons. In the welding process, the expulsion may occur at only a certain point in time. For that reason, most of the curves will appear "normal." A sharp drop of dynamic resistance could be observed in situation of expulsion [11]. However, in our experiment, due to manual operation of the welding machine and the absence of cooling system, the profile of dynamic resistance was significantly affected by various disturbanceS, and the resistance drop related to the expulsion was not identified from the signal. In light of the arguments presented above, the idea of sliding window was used again to identify features which could be related to the expulsion. The principle of the proposed SOM-type classifier is to make guesses of the features based on similarities and differences between the samples with and without expulsion.

Before the detailed description of the SOM-type classifier, we consider a simple case where for each time frame, only one neuron is assigned to

classify the expulsion condition. Each time frame has length of three and moves along the time series with overlapping. The adjacent three resistance data and three power data together construct the vectors for each time frame. The neurons have weight vectors of the same length as the vectors in each time frame. The purpose of the neurons is to find out the features that may be related to expulsion.

For samples without expulsion, each time interval along the time series was normal. As such, all the vectors can be considered as vectors unrelated to expulsion. Before the training process, all the vectors and their positions along their time series from the training samples with no expulsion were extracted and kept in a "good set".

In the training part, the weight vectors of neurons were initialized to be the mean positions of the vectors at the corresponding positions from the samples with expulsion in training set. In each iteration, a random sample with expulsion was chosen as the input. At each time frame, the Euclidean distance between the input vector and the vectors in the corresponding nearby positions from "good set" were compared. The minimum distance was considered as the distance of the input vector to the "good set" represented by D. The corresponding nearby positions also included the time frame ahead of the corresponding position and the time frame after the corresponding position. This was because for different welds, the welding

process might not be coherent. A simple example of D in two dimensions is shown in Figure 4.11.

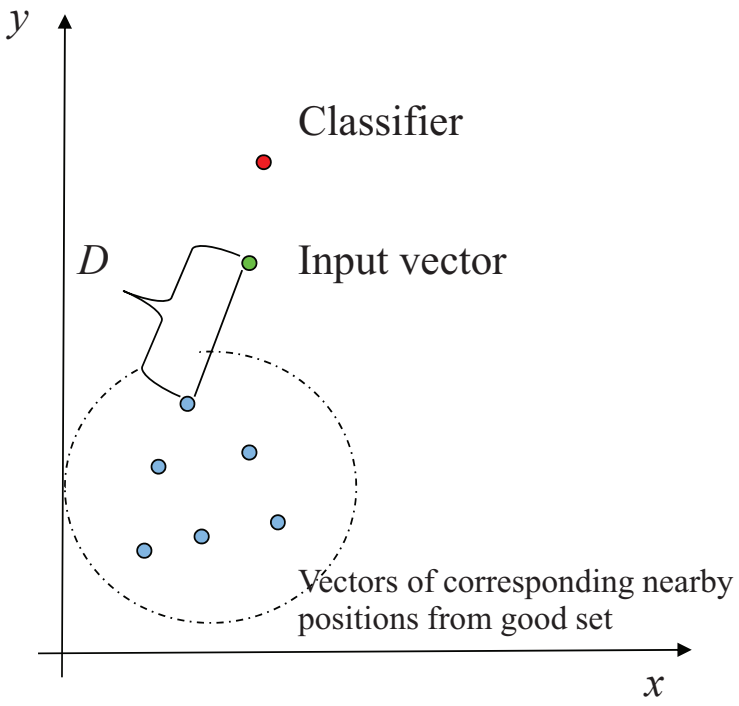

Figure 4.11: A simple example of the distance in two dimensions.

For each input sample, if at least one vector has a distance to the neurons 0.8 times shorter than to its corresponding D, the sample will be classified as a sample with expulsion. Otherwise, if none of the vectors appears to be nearer to the neurons, the sample is considered to have no expulsion and the classification is wrong. Adjustments are then required to be done to the neurons. Accordingly, all the neurons will be moved towards the vectors of the sample by

$$w(k+1) = (1 - D^2)w(k) + D^2 x, \tag{4.10}$$

where x represents the input vector. The movement is designed to be proportional to D^2 which means that the farther the input vector is from the good set, the more likely the neuron will trend to move towards the input vector. The learning rate is not involved in 4.10 because the values of D are all very small and they can work as learning rate. The training will continue until all the training samples with expulsion are classified correctly. After that, the trained neurons and good set are applied to the testing set to check the expulsion condition.

The method can be improved by assigning more neurons to each time frame, *e.g.*, five neurons. Correspondingly, the weight vectors for the neurons are initialized to be a random variation from the mean positions of the vectors at the corresponding positions from the training samples with expulsion. In each iteration, the neurons will compete with each other and the neuron with the smallest Euclidean distance to the input vectors of each time frame are chosen as the winner. Only winners will be updated in each iteration. Other than that, the training process is almost the same with (4.10). After the training part, the neurons that once were winners are chosen for the classification of the testing set.

This method can automatically "guess" the most possible features relating to expulsion according to the differences and similarities between the samples with expulsion and samples without expulsion. After that, the features are applied to classify samples based on their expulsion condition. This method is useful when strong noise corrupts the signals and the exact features relating to expulsion are unknown.

4.2 Experiment and Results

In this section, the design of the experiments to verify the proposed quality estimation scheme was discussed. The experimental setup and the quality evaluation parts were improved. As a result, the data acquisition was faster and more convenient. More aspects of quality were considered.

4.2.1 Experiment Setup and Procedure

To verify the effectiveness of proposed quality estimation scheme, thirty welds were conducted. The experimental setup was upgraded. The new setup is illustrated in Figure 4.12. A weld scanner was employed to replace the PC. An integrator called process sensor P100K was implemented so that the current signal can be integrated directly from the voltage signal measured by Rogowski coil. The current and voltage signals were connected to the process sensor P100K for preprocessing and the filtered

signals were directed to the weld scanner for recording and display. The implementations of weld scanner reduced the sampling rate resulting a sampling rate to around 3000 Hz.

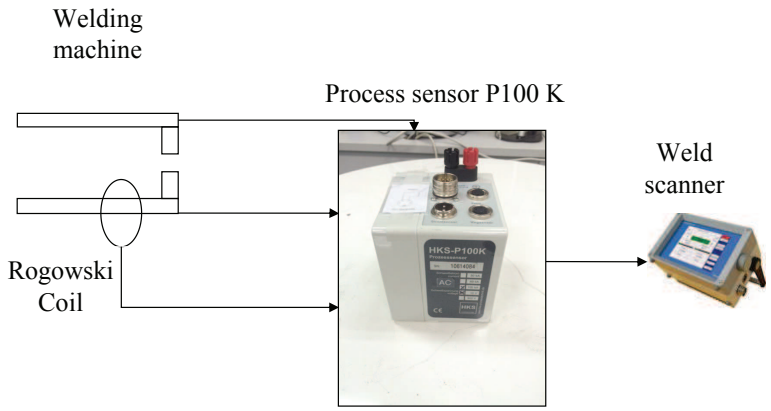

Figure 4.12: Experimental setup for the proposed quality estimation scheme.

The work pieces for the experiments were 1.2 mm and 2 mm thick galvanized steels of one inch wide and long. Thirty welds were conducted with ten welds of welding time 0.18 s, ten welds of 0.27 s, and ten welds of 0.44 s.

After welding, the quality of all the samples were examined carefully. More aspects of the quality of the samples were checked other than the expulsion condition using the nugget size the hte HAZ size. The detailed quality measurement procedure are shown in the following sections.

In order to check the various aspects of the qualities of the welded piece such as nugget size, HAZ size, and expulsion condition, the samples

were required to be open up to expose its cross sections as well as the faying surface. In general, the destructive process consists of five steps, photographing of indentation, cutting, curing, grinding and etching.

Photographing

First of all, the indentations of the samples were photographed and archived using a low magnification optical microscope. The image of indentation is shown in Figure 4.13. For convenience, the thin plate side is called the "surface" side, while the thick plate side is called the "bottom" side.

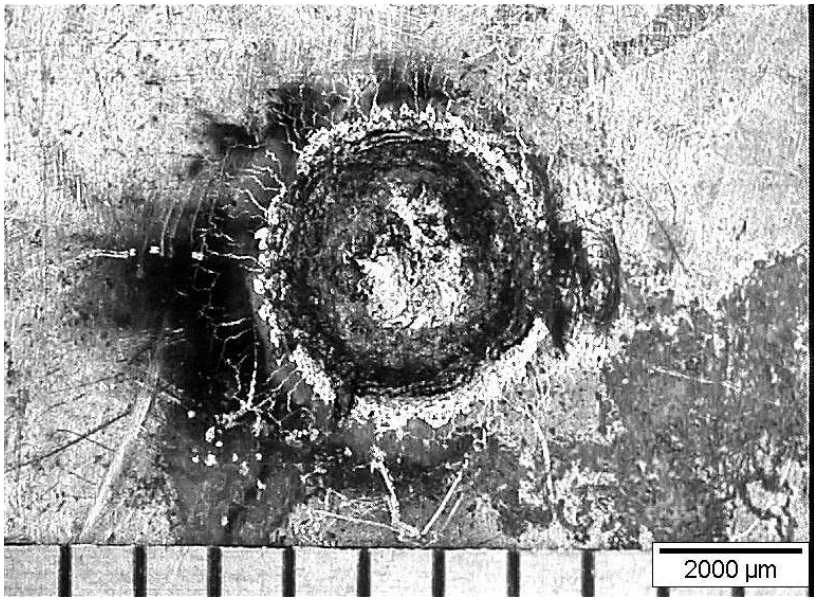

Figure 4.13: A picture of indentation.

From the images, it can be indicated that there are mainly three regions on the indentation. The white and shining region is the base material. Its property is unaffected by the welding process. The center circle area

appearing to be black with a shining ring is the mainly welding area. It is the resultant of the pressure of electrode and the melting of the surface material by the heat. The area around it has darker colors than the surrounding base material and is the HAZ. This is due to the change of microstructure by the heat passing by. The indentations on the surface side and bottom side happened to be of different sizes due to the difference of the thickness. For most of the samples, the main welding region and HAZ were not perfectly circular and expelling of metal was very common.

Cutting

In the second step, the samples were cut right at the edge of the nugget as illustrated in Figure 4.14.

Figure 4.14: Examples of how the samples were cut.

The remainding part was sent for curing and grinding to expose the cross-section right in the center of the nugget. The expulsion condition was indicated from the abandoned part. The comparison between the expulsion sample and non-expulsion sample from the abandoned part are shown in Figure 4.15.

Figure 4.15: Examples of sample with expulsion and sample without expulsion.

Curing

Curing was in the third step. The reminding part was mounted in a mould as shown in Figure 4.16. Epoxy hardener and Epoxy resins as shown in Figure 4.16 were mixed and poured into the mould. The curing took eight hours. After that, glass like finish was achieved for convenient grinding.

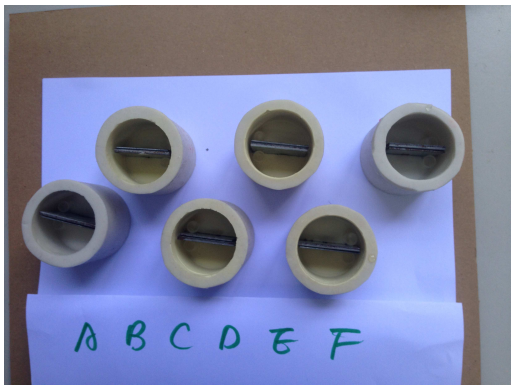

(a)

(b)

Figure 4.16: An illustration of (a) how the reminding part was mounted and (b) the chemicals for curing.

Grinding

In the fourth step, the samples were grinded by the grinding machine. A picture of the grinding machine was shown in Figure 4.17a. The roughest grinding paper disc was used firstly. The finer grinding papers were applied in sequence to finer grind the nugget until the center of the nugget was exposed. Polishing was done in the last part of grinding with the aid of the oil-based polishing solution as shown in Figure 4.17b.

After the grinding procedure, a mirror like cross section could be achieved. However, none of the fusion zone or the HAZ zone could be identified from the cross section. As such, etching was used to visualize various area.

Etching

The last step was etching. Natal (5%) (solution of alcohol and nitric acid) was applied to etch the cross section. The etching should be conducted in a fuming cupboard. In etching, one drop of Natal acid should be dropped onto the cross section. Next, the sample should be dipped into water very quickly to stop the reaction the moment a very slight color change appeared on cross section. Dipping the sample into the water too early or too late would result in under-etching or over-etching, respectively, leading to difficulty in spotting various regions clearly.

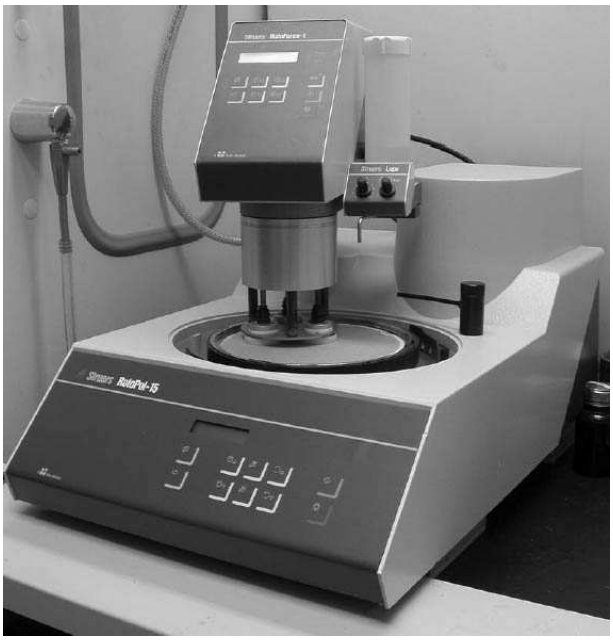

(a)

(b)

Figure 4.17: Pictures of (a) grinding machine and (b) the oil-based polishing solution.

After the etching, the fusion zone and HAZ could be visualized clearly under the low magnification optical microscope. An example of the cross section was shown in Figure 4.18. From Figure 4.18 it can be seen that the cross section was mainly composed of three zones, the fusion zone, the HAZ zone, and the base material. However, the boundary between the HAZ and the base material was still blurred. Moreover, the boundary between the fusion zone and the HAZ was even more blurred. This caused great difficulty in the measurement of nugget size and HAZ size. As compared to the nugget size, the HAZ is easier for measuring as the HAZ around the indentation had very clear boundary. Furthermore, it was obvious that the nugget size and HAZ size had strong positive correlation with each other. In order to enhance the precision, the HAZ size was measured and utilized as the main indicator of the quality of the welded pieces instead of using the nugget size. Considering the non-circular shape of HAZ zone around the indentation and the size difference between the face and bottom, the HAZ size for each sample was calculated as the average of all two perpendicular measurements of the diameters of HAZ on both the surface side and the bottom side. The expulsion condition and HAZ size of all the samples will be presented in the next section.

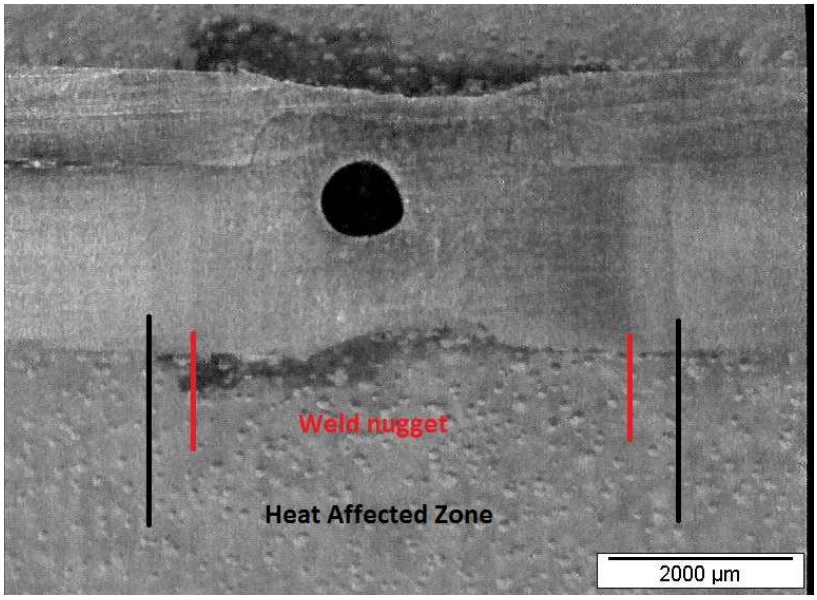

Figure 4.18: An example of the cross section.

4.2.2 Results and Discussion

In this section, the proposed quality estimation scheme was applied to estimate the HAZ size and expulsion condition of the welded samples. The performance of the proposed scheme was discussed and compared with the traditional multi-layer NN.

Estimation of HAZ Size

The HAZ sizes of all the samples from the experiments are shown in Table 4.1. The measured HAZ sizes of all the thirty samples are shown in Figure 4.19a. In general, it can be interpreted from Figure 4.19b that the HAZ became larger with longer welding time. The relationship between the welding time and HAZ size can be indicated by Figure 4.18.

The relationship was almost linear. However, the fluctuation of HAZ was notable which meant that other than the welding time, other parameters also had a marked influence on the HAZ size.

Table 4.1: The HAZ size of all the samples

Sample No.	HAZ size (mm)	Sample No.	HAZ size (mm)
1	6.3385	16	7.1533
2	6.4763	17	7.2637
3	6.4629	18	7.4674
4	6.4711	19	7.1718
5	6.0467	20	7.3370
6	6.1474	21	8.8908
7	6.2578	22	9.0516
8	6.4059	23	9.0604
9	5.9607	24	9.0039
10	5.8763	25	9.2417
11	7.3666	26	8.9269
12	7.4978	27	9.2007
13	7.2000	28	9.0936
14	7.1622	29	9.0107
15	7.4518	30	9.0497

To verify the performance of the proposed sliding window RNN in the estimation of HAZ size, a training set was created by randomly choosing five samples of welding time 0.18 s, five samples of welding time 0.27 s, and five samples of welding time 0.44 s. The rest of the samples constructed the testing set. The features selected in the proposed quality estimation

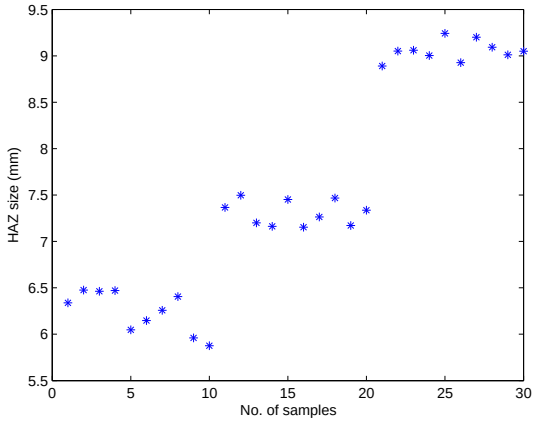

(a)

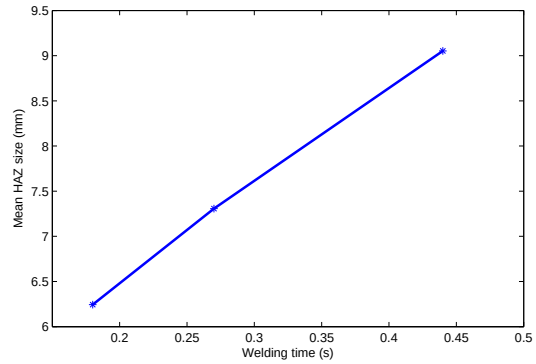

(b)

Figure 4.19: (a) The HAZ size of all the thirty samples; (b) The relationship between the HAZ size and welding time.

scheme were the peak powers and dynamic resistances at the instants of peak powers.

The proposed sliding window RNN was then applied. The NN had one hidden layers of twenty-four neurons. In the training process, the training set was fed into the sliding window RNN in random sequence for avoidance of bias. The training was stopped when the sum of squared error was below 0.001. The whole training process took around four hundred iterations and 200 s. In the testing process, the trained NN was applied to the testing set to estimate the HAZ size.

The comparison between the actual HAZ size and estimated HAZ size of both the training set and testing set was shown in Table 4.2 and Table 4.3. The results showed that the percentage error for most of the training samples were around 1%. The maximum percentage error was 2.05%. For testing samples, the percentage error fluctuated around 3% with maximum percentage error of 6.76%. The accuracy of estimation was satisfactory.

For comparison purpose, a simple multi-layer NN was used. The NN had only one hidden layer of twenty-four neurons. The whole time series of normalized dynamic power and normalized dynamic resistance were combined as the input vector. Due to the welding time difference, the dynamic power and dynamic resistance may have different length for different samples. To solve the problem, the vectors for powers and

Table 4.2: Comparison between the actual HAZ size and estimated HAZ size of the training set

Sample No.	Actual size(mm)	Estimated size (mm)	Percentage error
2	6.4763	6.4751	0.02%
3	6.4629	6.5225	0.92%
5	6.0467	6.0378	0.15%
9	5.9607	5.8238	2.3%
10	5.8763	5.8617	0.25%
11	7.3666	7.4325	0.89%
16	7.1533	7.2987	2.03%
18	7.4674	7.4769	0.13%
19	7.1718	7.2789	1.62%
20	7.3370	7.3682	0.67%
22	9.0516	8.9999	0.61%
26	8.9269	8.7979	1.3%
28	9.0936	9.1599	0.51%
29	9.0107	8.9905	0.51%
30	9.0497	9.0063	0.22%

Table 4.3: Comparison between the actual HAZ size and estimated HAZ size of the testing set

Sample No.	Actual size (mm)	Estimated size (mm)	Percentage error
1	6.3385	6.3398	0.02%
4	6.4711	6.5301	0.91%
6	6.1474	6.0375	1.79%
7	6.2578	6.6217	5.81%
8	6.4059	6.3189	1.36%
12	7.4978	7.0081	6.53%
13	7.2000	7.4233	3.1%
14	7.1622	7.3664	2.85%
15	7.4518	7.3748	1.03%
17	7.2637	7.7550	6.76%
21	8.8908	8.4910	4.5%
23	9.0604	8.7840	3.05%
24	9.0039	8.6972	3.41%
25	9.2417	8.8786	3.93%
27	9.2007	9.1959	0.05%

resistances were initialized separately to the maximum lengths among all the samples. For each sample, the missing points were set to zero. The power and resistance vectors were then combined in sequence as the input to the NN as

$$x_n = \begin{bmatrix} P_n(1) & P_n(2) & P_n(3) & ... & P_n(42) & r_n(1) & r_n(2) & r_n(3) & ... & r_n(42) \end{bmatrix}, \tag{4.11}$$

where n is the sample number. The accuracies for both training set and testing set were shown in Table 4.4 and Table 4.5. It was shown that the accuracy of estimation by simple multi-layer NN was much lower. The proposed sliding window RNN is more efficient and accurate in dealing with HAZ size of varying welding time. It also represents great usefulness of embedding NN into model of dynamic process.

The proposed sliding window RNN was also able to plot HAZ growth curve other than estimation of the final HAZ size. The HAZ curves of all the training samples are shown in Figure 4.20a. From Figure 4.20a, it can be easily noticed that the HAZ size increases very rapidly in the beginning. As time goes on, the increase will gradually slow down. The results corresponds well with the experimental results for nugget growth in [50] as shown in Figure 4.20b.

Table 4.4: Comparison between the actual HAZ size and estimated HAZ size of the training set

Sample No.	Actual size (mm)	Estimated size (mm)	Percentage error
2	6.4763	6.4708	0.09%
3	6.4629	6.4658	0.04%
5	6.0467	6.0383	0.14%
9	5.9607	5.9598	0.02%
10	5.8763	5.8838	0.13%
11	7.3666	7.3003	0.9%
16	7.1533	7.1601	0.09%
18	7.4674	7.5018	0.46%
19	7.1718	7.3191	2.05%
20	7.3370	7.2719	0.89%
22	9.0516	9.0646	0.14%
26	8.9269	8.8818	0.51%
28	9.0936	8.8849	2.29%
29	9.0107	9.0932	0.91%
30	9.0497	9.0793	0.33%

Table 4.5: Comparison between the actual HAZ size and estimated HAZ size of the testing set

Sample No.	Actual size (mm)	Estimated size (mm)	Percentage error
1	6.3385	7.3498	15.95%
4	6.4711	5.6958	11.98%
6	6.1474	5.2258	14.99%
7	6.2578	8.5173	36.11%
8	6.4059	7.3704	15.06%
12	7.4978	7.2236	3.66%
13	7.2000	7.4224	3.09%
14	7.1622	7.5281	5.11%
15	7.4518	8.056	8.11%
17	7.2637	7.9471	9.41%
21	8.8908	8.9450	0.61%
23	9.0604	9.0853	0.27%
24	9.0039	8.3445	7.32%
25	9.2417	9.0596	1.97%
27	9.2007	8.9388	2.85%

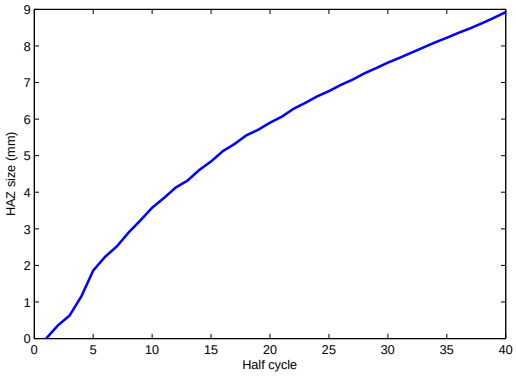

(a)

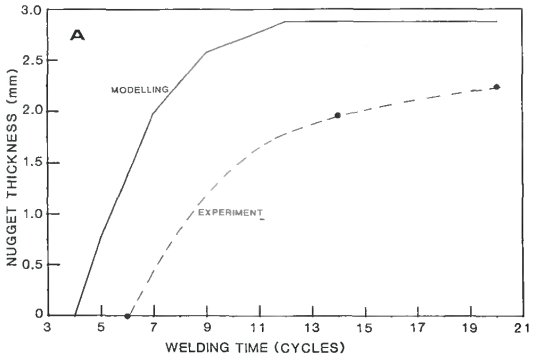

(b)

Figure 4.20: (a) The nugget growth curve estimated; (b) Nugget growth curve measured by experiment [50].

Classification of Expulsion Condition

The expulsion conditions of all the samples from the experiments are shown in Table 4.6. In summary, there were twelve samples with expulsion. In Figure 4.21, the signals from samples with and without expulsion are compared. It is shown that because of the fierce disturbance from the environment, it was very difficult to figure out a clear feature that could distinguish the two conditions. For that reason, the proposed SOM-type classifier was applied to learn from the similarity and difference of two categories of samples and classify the expulsion condition.

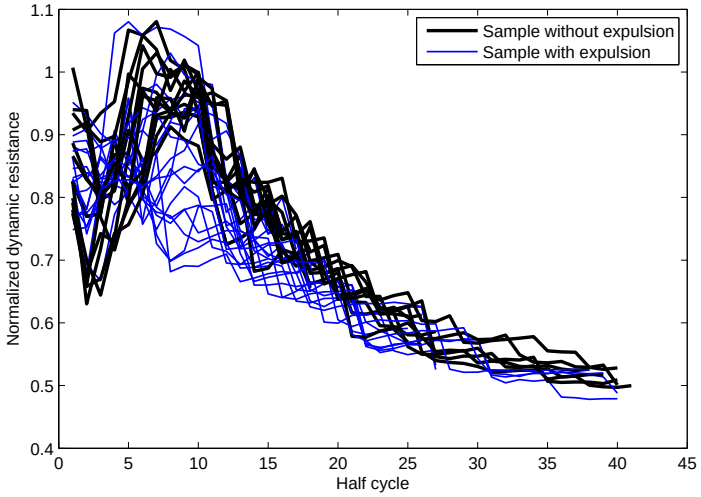

Figure 4.21: Comparison of dynamic resistance curves between sample with expulsion and sample without expulsion.

In the beginning, the performance of one neuron per time frame was tested. In the training part, nine samples without expulsion and six samples with expulsion were selected randomly for the training of the network. The

Table 4.6: Expulsion conditions of all the samples. Label 0: Sample without expulsion. Label 1: Sample with expulsion

Sample No.	Label	Sample No.	Label
1	0	16	0
2	0	17	0
3	1	18	1
4	1	19	0
5	0	20	0
6	1	21	1
7	0	22	1
8	0	23	0
9	0	24	0
10	0	25	1
11	1	26	0
12	0	27	1
13	0	28	1
14	1	29	1
15	0	30	0

Table 4.7: Comparison between the actual expulsion condition and estimated expulsion condition by SOM-type classifier with one neuron per time frame. Label 0: Sample without expulsion. Label 1: Sample with expulsion

Sample No.	Actual Label	Estimated Label
1	0	0
4	1	0
6	1	0
7	0	0
8	0	0
12	0	0
13	0	0
14	1	1
15	0	0
17	0	0
21	1	0
23	0	0
24	0	0
25	1	1
27	1	1

training was stopped when all the samples with expulsion were classified correctly. The test set was then fed in to evaluate the performance. The classification results were shown in Table 4.7.

From Table 4.7, it can be seen that Samples 4, 6, and 21 were wrongly classified as samples without expulsion. The overall accuracy reached 80%. Next, five neurons per time frame were used. The testing results are shown in Table 4.8. It is shown that only Sample 4 was misclassified and 14 out of 15 samples were classified correctly. The accuracy achieved was 93.33%.

For comparison, a simple multi-layer NN was also applied to check the expulsion condition. The NN had only one hidden layer of twenty-four

Table 4.8: Comparison between the actual expulsion condition and estimated expulsion condition by SOM-type classifier with five neurons per time frame. Label 0: Sample without expulsion. Label 1: Sample with expulsion

Sample No.	Actual Label	Estimated Label
1	0	0
4	1	0
6	1	1
7	0	0
8	0	0
12	0	0
13	0	0
14	1	1
15	0	0
17	0	0
21	1	1
23	0	0
24	0	0
25	1	1
27	1	1

Table 4.9: Comparison between the actual expulsion condition and estimated expulsion condition by multi-layer NN. Label 0: Sample without expulsion. Label 1: Sample with expulsion

Sample No.	Actual Label	Estimated Label
1	0	0
4	1	0
6	1	0
7	0	0
8	0	0
12	0	0
13	0	1
14	1	0
15	0	1
17	0	1
21	1	0
23	0	0
24	0	0
25	1	1
27	1	1

neurons. The input vector was formed by the dynamic power and resistance in the same way as the previous section. The classification results were shown in Table 4.9.

In Table 4.9, it is shown that seven samples were classified wrongly and the accuracy was only 53.33%. The accuracy was far below the classification using the SOM-type classifier. These results suggested that the SOM-type classifier was able to classify the expulsion condition with high accuracy in case that the dynamic resistance signals were severely corrupted by noise and no obvious features could be spotted.

4.3 Summary

In this chapter, the signal processing and artificial intelligence model for weld quality estimation, and the experiments were presented in detail. The proposed quality estimation scheme estimated HAZ size of welds of varying welding time with percentage error around 3% which surpassed the performance of traditional multi-layer NN. By using the SOM-type classifier, the expulsion conditions of the samples were classified with accuracy of up to 93.33%, while the traditional multi-layer NN only achieved 53.33%. In summary, the accuracy of the proposed scheme was much higher than the multi-layer NN method. Furthermore, by using the sliding window RNN, the HAZ growth curve was estimated and the trend corresponded well with the existing literature. For both methods, they show the capability to deal with welding of varying welding times.

Chapter 5

Conclusion and Future Work

Robust quality monitoring schemes of low costs and high accuracy are strongly needed in today's industry. This thesis proposed two schemes for the quality monitoring using advance feature extraction and artificial intelligence models. In view of experiments results, the following objectives have been achieved.

1. Only the easily obtainable electrical signals were used to classify the quality of spot welding. The current was measured by a Rogowski coil and the voltage was measured by connecting the two tongs of the welding machine to the data acquisition system. The method was very convenient, cheap, and flexible.

2. A fast and easy scheme using windowed feature extraction and SOM-based quality classification was proposed. The RMS current, RMS

voltage and dynamic resistance calculated using the RMS current and voltage were extracted from the captured electrical signals by sliding window-based feature extraction. Next, a SOM was applied to classify the quality of the samples using the extracted features. The scheme can classify the samples into no weld, good weld and weld with expulsion with fast speed and high accuracy. The training process took about 17.8 s and the overall accuracy reached 92.9%.

3. An improved scheme was proposed. The scheme used a sliding window RNN for estimation of HAZ size and a SOM-type classifier for expulsion checking. The estimation of the HAZ size achieved higher accuracy than a simple multi-layer neural network (NN). Meanwhile, the SOM-type classified the samples into samples with and without expulsion with an accuracy of up to 93.33%. In summary, the proposed schemes show great potential to cope with welds with varying welding time based only on electrical signals. Furthermore, the sliding window RNN presented the efficiency of using the NN in dealing with dynamic process. As for the proposed SOM-type classifier, it showed great usefulness in expulsion classification for signals severely corrupted by noise.

However, the proposed schemes should be further improved to enhance the robustness. In view of the results obtained, the following works should be emphasized in future research:

1. Improve robustness of SOM-type classifier:

   The accuracy of SOM-type classifier was highly dependent on initialization of neurons. With different initial values, the accuracy can vary in a very large range. As such, further modification of the SOM-type classifier is needed to stabilize the accuracy and make it more robust. Specific considerations on infinite horizon and mean position may be explored.

2. Generalize the sliding window RNN:

   Currently, only the change of welding time was covered in training the NN. In the future work, the situation of change of welding machine or change of welding material can be introduced to test the robustness of the NN under changes of experimental conditions. With more situations covered in training process, the trained NN can be used in more applications.

3. Verify the HAZ growth curve predicted by sliding window recurrent neural network (RNN) via experiments:

   The proposed sliding window RNN shows great potential in estimating the nugget growth curve. The estimated growth curve has

the same trend as the measured growth curve in existing literature. However, more experiments are required to be conducted to measure the nugget size during the welding experiments to verify if the estimation by proposed scheme is effective.

4. Introduce instrumental testing methods to quality estimation:

   In this thesis, the nugget size and the HAZ size were used as quality indicators. However, by using instrumental testing methods, the shear and tensile strengths can be measured and are more direct in showing the quality of welds in real application. The proposed schemes can also been used to estimated the shear and tensile strengths.

Bibliography

[1] European Aluminium Website [Online], The Aluminium Automotive Manual, *http://www.alueurope.eu/wp-content/uploads/2012/01 /AAM-Joining-2-Resistance-welding.pdf.*

[2] Z. D. Ishaya, M. Dauda, G. Y. Pam, and D. M. Kulla, "Destructive Testing and Production System Integrity," *Advances in Applied Science Research*, in press.

[3] A. Runnemalm and A. Appelgren "Evaluation of Non-destructive Testing Methods for Automatic Quality Checking of Spot Welds," *SpotLight*, in press.

[4] M. A. Javed and S. A. C. Sanders, "Neural Networks Based Learning and Adaptive Control for Manufacturing Systems," in *Proceedings of the 1991 IEEE/RSJ International Workshop on IROS*, pp. 242–246, Osaka, Japan, November 3–5, 1991.

[5] Polytechnic University Website [Online], Learning Vector Quantization, *http://cis.poly.edu/ mleung/CS6673/s09/LVQ.pdf*, 2009.

[6] Y. J. Cho and S. H. Rhee, "Quality Estimation of Resistance Spot Welding by Using Pattern Recognition with Neural Networks," *IEEE Transactions on Instrumentation and Measurement*, Vol. 53, No. 2, pp. 330–334, April 2004.

[7] E. B. Mahmoud, F. Dimitar, and B. C. Ratna, "Online Qualitative Nugget Classification by Using a Linear Vector Quantization Neural Network for Resistance Spot Welding," *The International Journal of Advanced Manufacturing*, Vol. 36, No. 3–4, pp. 237–249, March 2008.

[8] Power Electronic Measurements website [Online], *http://www.pemuk.com/how-it-works.aspx.*

[9] LEM DynAmp Inc. Website [Online], An Overview of Rogowski Coil Current Sensing Technology, *http://www.dynamp.com/ldadocum.nsf/c2270fbdd892ac3e86256e75000ad88a/e710af6d3e0f6255862565d7004b19db/$FILE/Report.pdf*, 2000.

[10] M. H. Samimi, A. Mahari, M. A. Farahnakian, and H. Mohseni, "The Rogowski Coil Principles and Applications: A Review," *IEEE Sensors Journal*, Vol. 15, No. 2, pp. 651–658, November 2014.

[11] P. Podrzaj, I. Polajnar, J. Diaci, and Z. Kariz, "Expulsion Detection System for Resistance Spot Welding based on a Neural Network," *Measurement Science and Technology*, Vol. 15, pp. 592–598, March 2004.

[12] J. Senkara, H. Zhang, and S. J. Hu, "Expulsion Prediction in Resistance Spot Welding," *Welding Journal–New York*, Vol. 83, No. 4, pp. 123S–132S, April 2004.

[13] C. P. Nex and R. A. Smith , "Impact Performance of Model Spot Welded Stainless Steel Structures," *Experimental Mechanics*, in press.

[14] R. Aamodt, "Using Artificial Neural Networks to Forecast Financial Time Series," *Master Thesis*, Norwegian University of Science and Technology, 2010.

[15] G. Mihalakakou, M. Santamouris, and D. Asimakopoulos, "Modeling Ambient Air Temperature Time Series Using Neural Networks," *Journal of Geophysical Research: Atmospheres*, Vol. 103, No. D16, pp. 19509–19517, August 1998.

[16] J. M. P. Junior, and A. B. Guilherme, "Multistep-Ahead Prediction of Rainfall Precipitation Using the NARX Network," in *Proceedings of the 2008 ESTSP*, pp. 87–96, Porvoo, Finland, September 17–19, 2008.

[17] R. J. Frank, N. Davey, and S. P. Hunt, "Time Series Prediction and Neural Networks," *Journal of Intelligent and Robotic Systemsm*, Vol. 31, No. 1–3, pp. 91–103, May 2001.

[18] M. P. Jose, J. Menezes, and G. D. A. Barreto, "A New Look at Nonlinear Time Series Prediction with NARX Recurrent Neural Network," in *Proceedings of the 2006 SBRN* , pp. 160–165, Ribeirao Preto, Brazil, Octorber 23–27, 2006.

[19] E. Diaconescu, "The use of NARX Neural Networks to Predict Chaotic Time Series," *WSEAS Transactions on Computer Research*, Vol. 3, No. 3, pp. 182–191, March 2008.

[20] A. G. Thakur, A. R. Rasane, and V. M. Nandedkar, "Finite Element Analysis of Resistance Spot Welding to Study Nugget Formation," *International Journal of Applied Engineering Research*, Vol. 1, No. 3, pp. 483–490, August 2010.

[21] H. A. Nied, "The Finite Element Modeling of the Resistance Spot Welding Process," *Welding Journal*, Vol. 63, No. 4, pp. 123–132, April 1984.

[22] C. L. Tsai, J. C. Papritan, D. W. Dickinson, and O. A. Jammal, "Modeling of Resistance Spot Weld Nugget Growth," *Welding Journal*, Vol. 71, No. 2, pp. 47–54, Feburary 1992.

[23] M. Rashid, J. B. Medley, and Y. Zhou, "Nugget Formation and Growth During Resistance Spot Welding of Aluminium Alloy 5182," *Canadian Metallurgical Quarterly*, Vol. 50, No. 1, pp. 61–71, January 2011.

[24] Resistance Welding Equipment and Supply Co. Website [Online], Resistance Spot Welding of Zinc Coated Steels, *http://www.rsfinishing.com/downloads/pdf/downloads_page/ZINC-COATED-STEELS.pdf*.

[25] S. A. Gedeon and T. W. Eagar. "Resistance Spot Welding of Galvanized Steel: Part II. Mechanisms of Spot Weld Nugget Formation," *Metallurgical Transactions B*, Vol. 17B, pp. 887–901, December 1986.

[26] M. Pouranvari, "Effect of Fusion Zone Size on the Mechanical Response of DQSK Steel Resistance Spot Welds," *Australian Journal of Basic and Applied Sciences*, Vol. 5, No. 12, pp. 573–577, December 2011.

[27] T. Kim, H. Park, and S. Rhee, "Optimization of Welding Parameters for Resistance Spot Welding of TRIP Steel with Response Surface Methodology," *International Journal of Production Research*, Vol. 43, No. 21, pp. 4643–4657, January 2005.

[28] R. S. Florea, D. J. Bammann, A. Yeldell, K. N. Solanki, and Y. Hammi, "Welding Parameters Influence on Fatigue Life and Microstructure in Resistance Spot Welding of 6061-T6 Aluminum Alloy," *Materials and Design*, Vol. 45, pp. 456–465, March 2013.

[29] D. Kianersi, A. Mostafaei, and J. Mohammodi, "Effect of Welding Current and Time on the Microstructure, Mechanical Characterizations, and Fracture Studies of Resistance Spot Welding Joints of AISI 316L Austenitic Stainless Steel," *Metallurgical and Materials Transactions A*, Vol. 45, No. 10, pp. 4423–4442, September 2014.

[30] M. Pouranvari, H. R. Asgari, S. M. Mosavizadch, P. H. Marashi, and M. Goodarzi, "Effect of Weld Nugget Size on Overload Failure Mode of Resistance Spot Welds," *Science and Technology of Welding and Joining*, Vol. 12, No. 3, pp. 217–225, April 2007.

[31] D. J. Radakovic and M. Tumuluru, "Predicting Resistance Spot Weld Failure Modes in Shear Tension Tests of Advanced High-strength Automotive Steels," *Welding Journal-New York*, Vol. 87, No. 4, pp. 96–105, April 2008.

[32] K. Feramuz, K. Ramazan, and G. Suleyman, "The Effect of Process Parameter on the Properties of Spot Welded Cold Deformed AISI304

Grade Austen," *Journal of Materials Processing Technology*, Vol. 209, No. 8, pp. 4011–4019, September 2009.

[33] Y. Purwaningrum and I. Chamid, "Critical Nugget Diameter of Resistance Spot Welded Stiffened Thin Plate Structure," *Modern Applied Science*, Vol. 7, No. 7, pp. 17–22, July 2013.

[34] D. Subramanian, G. K. Dongarkar, M. Das, V. Fernandez, and G. Grzadzinsky, "Real Time Monitoring and Quality Control of Resistance Spot Welds Using Voltage, Current, and Force Data," in *Proceedings of the 2004 International Conference on EIT*, pp. 211–220, Milwaukee, WI, August 26–27, 2004.

[35] Iowa State University Website [Online], Recursive Least Squares Estimation, *http://web.cs.iastate.edu/simcs577/handouts/recursive-least-squares.pdf*, 2014.

[36] Circuits and Systems Website [Online], Recursive Least Squares (RLS)-Chapter 9, *http://ens.ewi.tudelft.nl/Education/courses/et4235_new/slides/10_rls.pdf.*

[37] C. T. Ji and L. P. Deng, "Quality Control Based on Electrode Displacement and Force in Resistance Spot Welding," *Frontiers of Mechanical Engineering in China*, Vol. 5, No. 4, pp. 412–417, December 2010.

[38] H. Y. Zhang and J. Senkara, *Resistance Spot Welding Fundamentals and Applications*, CRC Press, Taylor and Francis Group, Boca Raton, FL, USA, 2013.

[39] M. Batista and S. D. Brandi, "Use Of Dynamic Resistance and Dynamic Energy to Compare Two Resistance Spot Welding Equipments for Automotive Industry in Zinc Coated and Uncoated Sheets," *American Journal of Engineering Research,* Vol. 02, No. 06, pp. 79–93, 2013.

[40] F. J. Garza and M. Das, "Identification of Time-Varying Resistance During Welding," in *Proceedings of the 2000 I2MTC*, Vol. 3, pp. 1534-1539, Baltimore, MD, May 1–4, 2000.

[41] C. M. Bishop, *Neural Networks for Pattern Recognition*, Oxford university press, UK, 1995.

[42] Y. M. Tan, P. Fang, Y Zhang, and S. Q. Yang, "Evaluating Nugget Sizes of Spot Welds by Using Artificial Neural Network," *Computational Intelligence*, Vol. 1625, pp. 53–58, 1999.

[43] T. Arunchai, K. Sonthipermpoon, P. Apichayakul, and K. Tamee, "Resistance Spot Welding Optimization Based on Artificial Neural Network," *International Journal of Manufacturing Engineering*, in press.

[44] J. Hertz, A. Krogh, and R. G. Palmer, *Introduction to The Theory of Neural Computation*, Addison-Wesley Publishing Company, Boston, USA, 1991.

[45] R. Zurita-Milla, J. A. E. van Gijsel, N. A. S. Hamm, P. W. M. Augustijn, and A. Vrieling, "Exploring Spatiotemporal Phenological Patterns and Trajectories using Self-organizing Maps," *IEEE Transections on Geoscience and Remote Sensing*, Vol. 51, pp. 1914–1921, November 2012.

[46] University of Birmingham Website [Online], Self Organizing Maps: Fundamentals, *http://www.cs.bham.ac.uk/∼jxb/NN/l16.pdf*, 2004.

[47] Y. M. Wang, A. Peyls, Y. Pan, L Claesen, and X. L Yan, "A Fast Self-organizing Map Algorithm for Handwritten Digit Recognition," *Multimedia and Ubiquitous Engineering*, Springer Netherlands, Vol. 240, pp. 177–183, May 2013.

[48] A. M. Salem, M. M. Syiam, and A. F. Ayad, "Improving Self-Organizing Feature Map (SOFM) Training Algorithm using K-means Initialization," in *Proceedings of the 2003 International Conference on ICEIS*, Vol. 40, pp. 41–46, Angers, France, April 23–26, 2003.

[49] PHM Society Website [Online], A Tutorial on Feature Extraction Methods,

https://www.phmsociety.org/sites/phmsociety.org/files/Tutorial_PHM12_Wang.pdf.

[50] American Welding Society Website [Online], An Examination of Nugget Development during Spot Welding, Using Both Experimental and Analytical Techniques, *https://app.aws.org/w/r/wj/supplement/WJ_1987_01_s1.pdf*, 1987.

[51] S. Duffner and C. Garcia, "An Online Backpropagation Algorithm with Validation Error-Based Adaptive Learning Rate," in *Proceedings of the 2007 Artificial Neural Networks-ICANN*, pp. 249–258, Porto, Portugal, September 9–13, 2007.

[52] P. R. Ji, Yichang, P. Wang, Q. Zhao , and L. Zhao, "A New Parallel Back-propagation Algorithm for Neural Networks," in *Proceedings of the 2011 IEEE International Conference on GSIS*, pp. 807–810, Nanjing, China, September 15–18, 2011.

[53] M. Moreira and E. Fiesler, "Neural Networks with Adaptive Learning Rate and Momentum Terms," *IDIAP Technique Report*, in press.

[54] R. Rojas, *Neural networks*, Springer-Verlag, Berlin, 1996.

[55] T. Kohonen, "Self-Organized Formation of Topologically Correct Feature Maps," *Biological Cybernetics*, Vol 43, No. 1 , pp 59–69, January 1982.

[56] X. J. Wang, J. H. Zhou, and C. K. Pang, "Feature Extraction for Classification of Welding Quality in RSW Systems," in *Proceedings of the 2014 IES*, Vol. 2, pp. 307–318, Singapore, November 10–12, 2014.

Curriculum Vitae

Wang Xingjue received his Bachelor of Science (Hons) degree in Applied Physics from Nanyang Technological University in January 2012. From January 2014 to August 2015, he is pursuing a Master of Engineering degree by research in Electrical and Computer Engineering in NUS. His current research interests include spot welding, signal processing and neural network. His research work related to this dissertation resulted in the following publications:

1. X. -J. Wang, J. -H. Zhou, and C. K. Pang, "Feature Extraction for Classification of Welding Quality in RSW Systems," in *Proceedings of the 2014 IES*, Vol. 2, pp. 307–318, Singapore, November 10–12, 2014.

2. X. -J. Wang, J. -H. Zhou, H. -C. Yan, and C. K. Pang, "Quality Monitoring of Spot Welding with Advanced Signal Processing and Data-Driven Techniques," submitted to *IET Control Theory and Applications*, September 2015.

3. X. -J. Wang, J. -H. Zhou, H. -C. Yan, and C. K. Pang, "Spot Welding Quality Monitoring with Advanced Signal Processing and Artificial Intelligence Models," to be submitted to *Proceedings of the 2016 IEEE IECON*, Florence, Italy, October 23-26, 2016.

His other publication include:

1. H. Y. Xu, X. -J. Wang, T. Y. Yu, H. D. Sun, and B. L. Zhang, "Radiation-Suppressed Plasmonic Open Resonators Designed by Nonmagnetic Transformation Optics," *Scientific Reports,* in press.